Linköping Studies in Science and Technology.
Licentiate Thesis No. 1590

Strength analysis and modeling of hybrid composite-aluminum aircraft structures

Zlatan Kapidžić

Linköping University
INSTITUTE OF TECHNOLOGY

LIU–TEK–LIC–2013:24

Division of Solid Mechanics
Linköping University, SE–581 83, Linköping, Sweden

Linköping, May 2013

Cover:
The picture illustrates the results from a finite element simulation of a hybrid structure, including local and global fastener joint failure.

Printed by:
LiU-Tryck, Linköping, Sweden, 2013
ISBN 978-91-7519-628-2
ISSN 0280-7971

Distributed by:
Linköping University
Department of Management and Engineering
SE–581 83, Linköping, Sweden

This document was prepared with LaTeX, April 30, 2013

Preface

The work presented in this Licentiate in Engineering thesis has been carried out at Saab AB and at the Division of Solid Mechanics, Linköping University. The work has been performed within the project FoT-Flygteknik: Optimalt utnyttjande av avancerade strukturmaterial i hybrida skrovkonstruktioner - HYBRIS, and was funded by Swedish Defense Material Administration (FMV) and Saab AB.

First, I would like to thank my supervisors, Hans Ansell (Saab AB) and Professor Larsgunnar Nilsson, for all their support and guidance during the course of this work. For valuable discussions and comments on my work I would like to thank all my colleagues within HYBRIS project and in particular Anders Bredberg (Saab AB). Also, I would like to thank all my colleagues at Saab AB and Linköping University for their help, encouragement and interesting discussions.

I am also grateful to my family and all my friends for their support. Especially, I would like to thank my dear Karin and my son Adrian for their patience and daily encouragement.

Linköping, May 2013

Zlatan Kapidžić

Abstract

The current trend in aircraft design is to increase the proportion of fiber composites in the structures. Since many primary parts also are constructed using metals, the number of hybrid metal-composite structures is increasing. Such structures have traditionally often been avoided as an option because of the lack of methodology to handle the mismatch between the material properties. Composite and metal properties differ with respect to: thermal expansion, failure mechanisms, plasticity, sensitivity to load type, fatigue accumulation and scatter, impact resistance and residual strength, anisotropy, environmental sensitivity, density etc. Based on these differences, the materials are subject to different design and certification requirements. The issues that arise in certification of hybrid structures are: thermally induced loads, multiplicity of failure modes, damage tolerance, buckling and permanent deformations, material property scatter, significant load states etc. From the design point of view, it is a challenge to construct a weight optimal hybrid structure with the right material in the right place. With a growing number of hybrid structures, these problems need to be addressed.

The purpose of the current research is to assess the strength, durability and thermo-mechanical behavior of a hybrid composite-aluminum wing structure by testing and analysis. The work performed in this thesis focuses on the analysis part of the research and is divided into two parts. In the first part, the theoretical framework and the background are outlined. Significant material properties, aircraft certification aspects and the modeling framework are discussed. In the second part, two papers are appended. In the first paper, the interaction of composite and aluminum, and their requirements profiles, is examined in conceptual studies of the wing structure. The influence of the hybrid structure constitution and requirement profiles on the mass, strength, fatigue durability, stability and thermo-mechanical behavior is considered. Based on the conceptual studies, a hybrid concept to be used in the subsequent structural testing is chosen. The second paper focuses on the virtual testing of the wing structure. In particular, the local behavior of hybrid fastener joints is modeled in detail using the finite element method, and the result is then incorporated into a global model using line elements. Damage accumulation and failure behavior of the composite material are given special attention. Computations of progressive fastener failure in the experimental setup are performed. The analysis results indicate the critical features of the hybrid wing structure from static, fatigue, damage tolerance and thermo-mechanical points of view.

List of Papers

The following papers have been included in this thesis:

I. Z. Kapidžić, L. Nilsson, H. Ansell, (2013), *Conceptual studies of a composite-aluminum hybrid wing box demonstrator*, Submitted.

II. Z. Kapidžić, L. Nilsson, H. Ansell, (2013), *Finite element modeling of mechanically fastened composite-aluminum joints in aircraft structures*, Submitted.

Note

The papers have been reformatted to fit the layout of the thesis.

Author's contribution

I have borne primary responsibility for all work presented in the papers included in this thesis.

The work in this project has also resulted in the following paper which is not included in this thesis:

I. Z. Kapidžić, R. Gutkin, (2013), *Detailed modeling of low velocity impact on a hybrid wing box structure*, Submitted to 4:th CEAS Air & Space Conference, September 16-19, 2013.

Contents

Preface **iii**

Abstract **v**

List of Papers **vii**

Contents **ix**

Part I – Theory and Background **1**

1 Introduction **3**
1.1 HYBRIS-project 5

2 Material characterization **9**
2.1 Static strength and stiffness 10
2.2 Fatigue damage development 14

3 Certification of aircraft structures **19**
3.1 Analysis 19
3.2 Testing 22

4 Constitutive modeling **25**
4.1 Elastic behavior 25
4.2 Failure criteria 28
4.2.1 Limit criteria 29
4.2.2 Polynomial criteria 29
4.2.3 Physically based criteria 30
4.3 Damage progression 33

5 Finite element modeling **37**
5.1 Modeling of bolted joints 37
5.2 Structural modeling 40

6 Outlook **45**

7 Review of included papers **47**

Bibliography **49**

Part II – Included papers **55**

Paper I: Conceptual studies of a composite-aluminum hybrid wing box demonstrator 59

Paper II: Finite element modeling of mechanically fastened composite-aluminum joints in aircraft structures 83

Part I

Theory and Background

1 Introduction

Aluminum alloys have, for a long time, been the primary materials used in aircraft structural design. Compared to most other metals, aluminum alloys have a high strength-to-weight ratio, which is essential for the aircraft performance and load-carrying capability. Aluminum alloys are, however, susceptible to fatigue and this poses a problem considering that aircraft structures usually are exposed to a large number of cyclic load repetitions during their operational life. The progress in material sciences and experimental techniques during the last century, as well as development of spectrum fatigue analysis, fracture mechanics and crack growth analysis, have advanced the knowledge of fatigue in metals and today the phenomenon is reasonably well-understood. Based on this knowledge, the aircraft industry has developed methods for securing the fatigue durability, the damage growth tolerance and the static and residual strength of aircraft metal structures with the aim of certifying their airworthiness and ensuring their structural integrity.

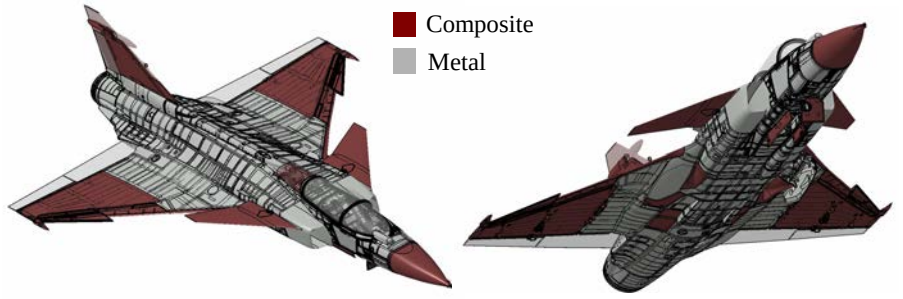

Figure 1: Composite and metal materials in JAS39 Gripen.

During the last three decades, the use of advanced light weight-high strength fiber reinforced polymers (FRP) composite materials in modern aircraft structures has rapidly increased [1]. For instance, about 20% of the JAS39 Gripen structure is made of FRP composite material, see Fig. 1. Based on the inherent property differences between the composites and metals [2], other certification and design methods adapted to the composites, had to be developed. Special attention was payed to the fact that composite laminates are sensitive to out-of-plane stresses, impact, environmental influence, and that they exhibit a multiplicity of failure

modes both in static and cyclic loading. The designs resulting from these methods were typically composite laminate panels that were sized to experience low in-plane strains and no, or very small, out-of-plane and interlaminar stresses. These design precautions are the reason why so few in-service composite fatigue failures have been reported and why the composites have gained a reputation of being fatigue insensitive.

With an increasing proportion of composite, the number of interfaces between metals and composites is growing. Structural parts that are made of both metal and composite materials and that include such interfaces are referred to as *hybrid structures*. Such mixed solutions have traditionally often been avoided as an alternative, because of the lack of a proper methodology to handle the mismatch of the material properties. But with a growing number of hybrid structures, this problem needs to be addressed. Some examples of differences between the properties of composite laminates and aluminum alloys are: thermal expansion coefficients, failure and fracture mechanisms, degree of plasticity, response to different types of loading, i.e. tensile versus compressive and out-of-plane, fatigue accumulation and scatter, impact resistance, impact residual strength, degree of anisotropy, environmental sensitivity, density etc. Based on these differences, composite and aluminum materials used in aircraft structures are subject to different design and airworthiness requirements. The issues that therefore arise with hybrid structures are: thermally induced stresses and deformations, multiplicity of failure modes in joints, unanticipated structural failure modes, allowance of buckling and permanent deformations, determination of testing factors to account for material property scatter, determination of significant load states etc. From a design point of view it is a challenge to construct a weight optimal hybrid structure, where the right material is put into the right place.

The recommended practice for certification of composite assemblies, known as the Building Block Approach (BBA) [3], [4], is to conduct analysis and testing at various levels of structural complexity. Usually, a large number of small specimens are tested and analyzed initially before progressing to more complex and expensive structural components, and finally ending with the test of the complete assembly. The knowledge gained at the previous levels is used as the base for designing the testing on the next level. In this way, the risks in technology associated with complexity of composites may be uncovered and eliminated at an early stage. When it comes to hybrid structures this approach may not always be appropriate, since the hybrid effects might be absent on lower structural levels. By this way of reasoning, the analyzes and tests should be performed on a higher level first, in order to evaluate the hybrid nature of a structure and to discover the unanticipated structural behavior. Such testing can be very costly and a lot of understanding can be gained by performing detailed numerical analyzes prior to the testing. For that purpose, structural modeling techniques that include damage accumulation and failure progression need to be developed. Some typical structural features that create a modeling challenge and a need for research are: bolted and bonded joints, holes, ply drop-off regions, delaminations and imperfections, impact dam-

ages, buckling panels etc. At Saab AB in Linköping and FOI in Stockholm, such research is conducted in the industrial project HYBRIS and this thesis is entirely based on the work performed within that project.

1.1 HYBRIS-project

The aim of the HYBRIS project is to assess the behavior of a hybrid wing-like box, with skins made of carbon fiber reinforced polymer (CFRP) and the inner structure made of aluminum, by testing and analysis. The material and geometry configuration of the object of study is based on the typical features of the real wing structure of Gripen aircraft, see Figs. 2 and 3. The structure is built of C-shaped spars and ribs bolted in a central splice section.

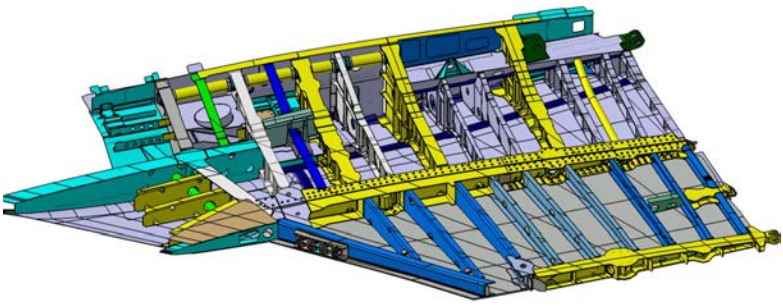

Figure 2: Wing structure of the JAS39 Gripen aircraft.

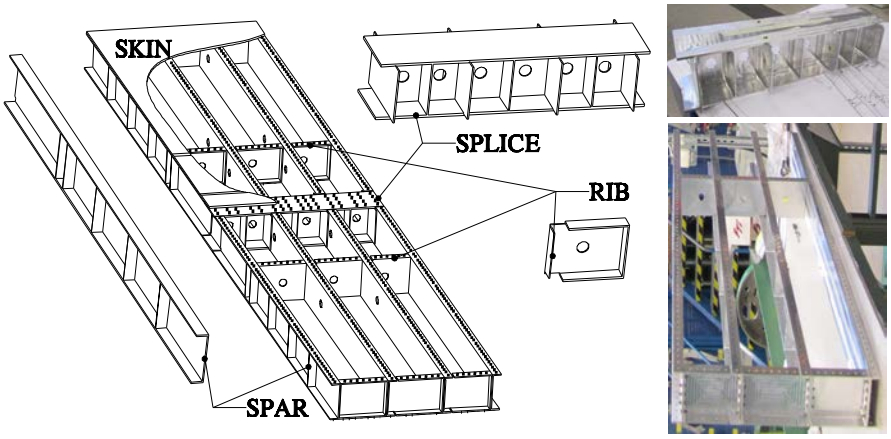

Figure 3: HYBRIS wing box with dimensions 3300x630x150 [mm].

The wing structure is normally exposed to bending and twisting operational loads and temperatures between -40°C and 80°C. To simulate this loading on the wing box, static and spectrum fatigue testing in a four point bending/twisting set up with an applied temperature is performed. Besides of its hybrid features, the wing box contains skin defects such as artificial delaminations, low velocity impact damages and different types of ply drop-off regions. Also, the dimensioning requirements used for composites, currently used in the industry, are modified for the purpose of challenging the conservative assumptions and allowables. At the end of the test program, the wing box will be filled with water and fired at with a small caliber bullet to test its battle damage resistance. The test results are expected to indicate the critical features of the hybrid box from static, fatigue and damage tolerance point of view. Also, the influence of thermally induced loads on the structural behavior should be revealed. Prior to the testing, the following analysis of the test object are performed: conceptual studies of different hybrid solutions and requirements, dimensioning analysis, local and global analysis of composite-aluminum bolted joints, impact analysis and virtual test simulation of the entire test object. This thesis work deals with parts of the analysis and modeling work related to the conceptual studies and modeling of bolted joints in the test object.

In the conceptual studies, two different cross-section designs of a hybrid wing box structure, without the splice section, are studied. The structure is designed given the thermal and mechanical loads and with respect to current requirements for static strength, fatigue and stability. The structural response, the local and global failure modes and the resulting weights of the two concepts are compared. Then the requirements concerning allowable strains, allowable buckling load and given thermal loads are modified and another comparison is preformed. Finally, one of the concepts is chosen for testing. The work concerning conceptual studies is appended in Paper 1.

In appended Paper 2, the wing box to be used in testing, Fig. 3, is modeled and analyzed using the finite element method (FEM). Special attention is payed to the shear loaded bolted joints present in the structure. A methodology is developed in which the local joint behavior, including damage accumulation in composite and metal plasticity, is assessed first. This behavior is then assigned to the structural elements representing the bolts in the global model of the wing box. Simulations with applied thermal and mechanical loads in the test setup are performed and the progressive failure of bolted joints is studied.

Certification of aircraft structures is, even without effects of hybrid structures, a very complex matter with a lot of different aspects and challenges. More efforts in the development of methodologies, modeling tools, testing strategies and further research of material and interface behavior are required to obtain more efficient and robust structures. The work performed in this project and presented in this thesis, as well as the activities planned for the future research, are a small step in this direction.

The thesis is outlined as follows. Chapter 2 describes the material characteristics

of CFRP and aluminum alloys that are relevant for understanding of the hybrid structure behavior. In Chapter 3 the certification procedure of aircraft structures is outlined. Chapter 4 discusses the constitutive modeling with focus on composite material behavior. In Chapter 5 some aspects of the numerical modeling of bolted joints and structures are discussed. In Chapter 6 future research topics are outlined and in Chapter 7 a review of the appended papers is made.

2 Material characterization

This chapter presents and compares the mechanical and thermal properties of CFRP composite laminates and aluminum alloys commonly used in aircraft structures. The aim is to highlight the differences and the incompatibilities of the two material types from the certification point of view.

The purpose of the certification of aircraft structures is to ensure their *structural integrity* and *durability*. These terms are closely related to concepts of *failure*, *fracture* and *damage* accumulation. This terminology is frequently used throughout this work and will therefore be briefly clarified.

Structural integrity can be described as the ability of the structure to perform the intended function and remain intact under the application of loads [5]. If the structure no longer is able to perform its intended function, *failure* has occurred, which means that the load-bearing capacity is lost or heavily reduced. For composite materials, in contrast to metals, failure does not necessarily mean that the structure no longer is intact or broken. In fact, composites can be exposed to considerable stiffness degradation to the point where they are non longer functional, but are still carrying significant loads and remaining intact. The term failure signifies a process, which is often divided in stages of initiation, progression and final failure stage. Failure is thus not equivalent to *fracture*. Fracture takes place when material breaks so that new internal surfaces are created. This could mean breaking up in two pieces or cracking locally, but it is often related to formation and growth of distinct cracks. In contrast to fracture, the term *damage* is used to refer to distributed, irreversible changes in the material that are governed by energy dissipating mechanisms. For example, metal damage can refer to plasticity or fatigue damage, and in composites it could be distributed matrix cracking or fiber breakage.

Durability is closely related to structural integrity and is defined as the ability of the structure to retain adequate properties (strength, stiffness and environmental resistance) throughout its life to the extent that any deterioration can be controlled and repaired [3].

With these definitions in mind, the properties of CFRP composite laminates and aluminum alloys are compared next.

2.1 Static strength and stiffness

Aluminum alloys used in aircraft structure applications are typically AA 2000 or AA 7000 series. Compared to most other metals these alloys have low density and relatively good strength and toughness, which is why they were, and still are, widely used by the aircraft industry. Good machinability of the material generally allows aluminum parts to be manufactured in almost any shape. Mechanical and thermal expansion properties of aluminum alloys are, on the macroscopic level, commonly considered to be homogeneous and in most cases even isotropic. Temperature deviations under 100°C from room temperature have only a moderate influence on the strength and stiffness properties of aluminum alloys [6]. When exposed to increasing static loading, aluminum alloys exhibit a linear stress-strain relation until the onset of plasticity. Thereafter, considerable plastic deformations and stress redistribution take place until final failure. On the micro-mechanical level, the plastic behavior of metals is governed by irreversible dislocation movement within their crystalline structure. The plasticity of metals is a quite well understood phenomenon with an established modeling framework and will not be discussed in detail in this thesis. Detailed descriptions of governing mechanisms and modeling techniques can be found in [7]-[9].

A typical FRP composite laminate consists of several unidirectional layers (also known as plies or laminae) of fiber reinforced polymer resin, stacked in different directions on top of each other and bonded by curing, see Fig. 4.

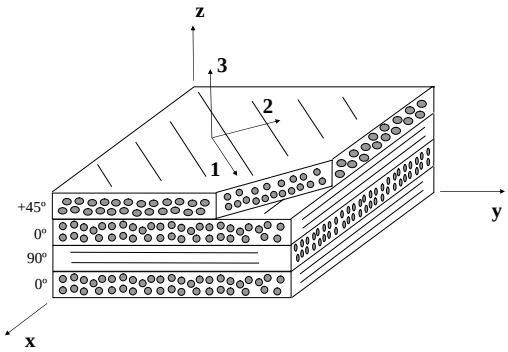

Figure 4: Composite laminate with local and global coordinate systems.

The laminate is most often cured directly into the shape of the final product. Depending on the laminate stacking sequence, different degrees of anisotropy are achieved. This can be exploited to tailor the laminate stiffness properties to suit the particular application. Generally, composite laminates have a higher strength-to-weight ratio than aluminum and almost a negligible thermal expansion coefficient. On the other hand, the strength of FRP laminates is sensitive to the influence of temperature and moisture content. Each lamina in itself is a non-homogeneous

composition consisting of fibers embedded in a polymer matrix. Despite this fact, most of the theoretical material models are based on the assumption that each fiber reinforced ply can be treated as homogeneous and orthotropic.

Unidirectional FRP composites, i.e. single ply composites, typically exhibit a linear stress-strain relation in the longitudinal (1-dir, parallel to the fiber direction) and transverse (2-dir, perpendicular to the fiber direction) loading directions until onset of failure, [10]-[12]. The in-plane shear stress-strain relation is non-linear due to the plastic deformation of the matrix [10], [13], [14]. However, in multiple layer composites the effect of the shear non-linearity is often limited, since the laminates are normally designed to be *fiber controlled*, which means that most of the load is transferred by the fibers. A comparison of stress-strain diagrams of a typical aluminum alloy [6] and a unidirectional CFRP composite [3] in longitudinal, transverse and shear loading is shown in Fig. 5. The fundamental differences in the stiffness and strength properties of aluminum and unidirectional CFRP composites are evident. When it comes to multidirectional laminates, however, the strength, the stiffness and the degree of anisotropy of the material depend on the lay-up sequence.

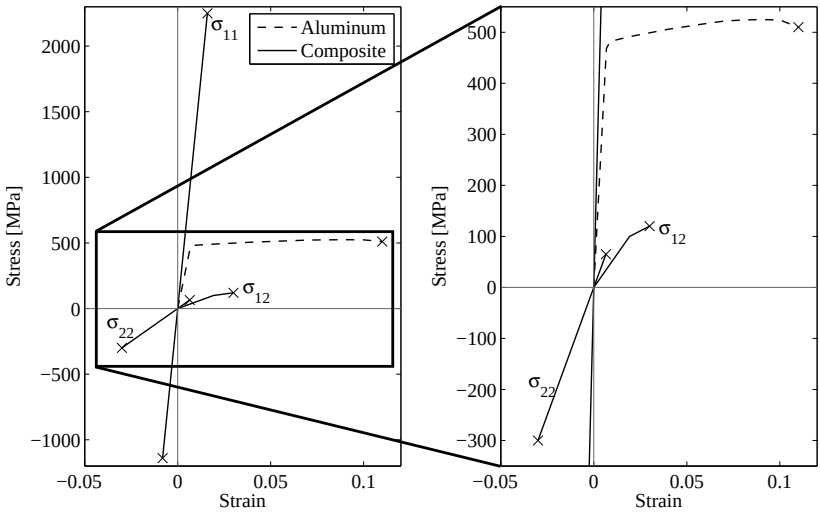

Figure 5: Comparison of stress-strain diagrams of aluminum alloy 7075-T6 and unidirectional composite HTA7/6376.

Also the damage accumulation and failure progression behavior of an FRP laminate are influenced by its heterogeneous characteristics. In contrast to aluminum, composite materials exhibit several different micro-mechanical damage modes depending on the loading situation [5], [11], [12]. They can be divided into two main categories: *intralaminar* (within a lamina) and *interlaminar* (between laminae) damage modes.

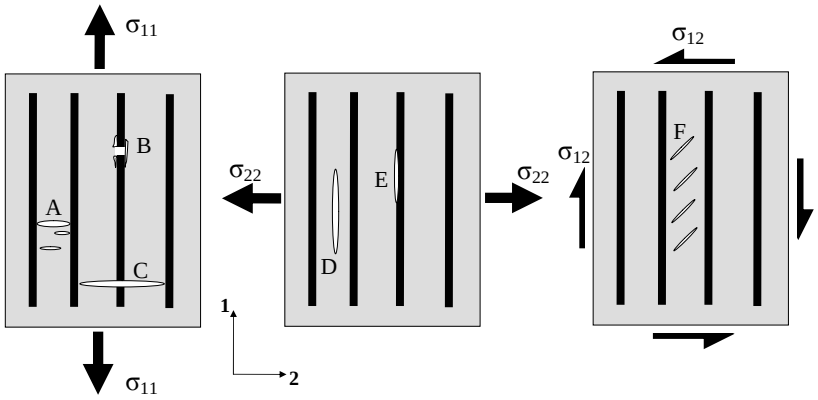

Figure 6: Intralaminar damage modes in longitudinal (1-dir) tensile, transverse (2-dir) tensile and in-plane shear loading. A) Matrix cracking. B) Fiber fracture with weak fiber/matrix interface. C) Fiber fracture with strong fiber/matrix interface and brittle matrix. D) Matrix cracking. E) Fiber/matrix interfacial debonding. F) Matrix cracking.

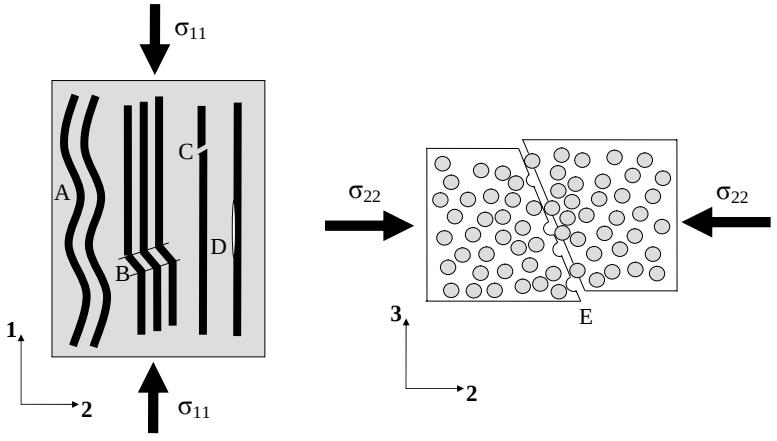

Figure 7: Intralaminar damage modes in longitudinal (1-dir) and transverse (2-dir) compressive loading. A) Elastic micro-buckling. B) Plastic micro-buckling and kink-band formation. C) Fiber shear fracture. D) Fiber/matrix interfacial debonding. E) Matrix shear fracture under compressive load.

Tensile longitudinal and transverse loading to the fiber direction and in-plane shear loading within a lamina result in intralaminar damage modes [15], [16], as shown in Fig. 6. The lamina strength in tensile loading in the longitudinal direction is mainly determined by the strength of the fibers, which makes this a fiber dominated failure

mode. This strength is usually very high in CFRP laminae, see Fig. 5. Similarly, transverse and shear loading give rise to matrix dominated failure modes. Transverse and shear lamina strengths are much lower then the longitudinal strength. In a bi-axial stress state the failure modes might interact and thereby accelerate the crack initiation and growth.

Longitudinal and transverse compressive loading on lamina level give different failure modes than those in the tensile cases, see Fig. 7. Fiber-buckling or kinking is usually triggered at the material point where an initial misalignment of the fibers is present [17]. The progression of the damage depends on the plasticity properties of the matrix and brittleness of the fibers. Since the fiber buckling load is much lower than the tensile strength of fibers, the resulting longitudinal lamina compressive strength is significantly lower than its longitudinal tensile strength. In compressive transverse loading, the cracking is driven by shear stresses on an inclined plane through the matrix and the fiber/matrix interfaces. The normal stress acting on this plane is compressive, which impedes the shear failure [18]. Consequently, the transverse compressive lamina strength is higher than the tensile and shear strength [10]. Both longitudinal and transverse compressive failure is promoted by a simultaneous presence of an applied shear stress [18].

Damage accumulation and failure behavior of multidirectional laminates are even more complex than those of a single lamina. The plies in multiple layer laminates are subjected to different local stress states which result in different damage and failure modes in different plies. As a result, the failure of plies within a laminate does not occur simultaneously, but in a progressive way. The presence of neighboring plies can also affect the damage initiation and growth within each embedded lamina. For instance, matrix crack growth is restricted by the neighboring plies, which increases the transverse strength of the embedded laminae, an effect known as the *in-situ* effect [19]. Another laminate specific failure mode is the *interlaminar* failure mode. As the name implies, this kind of failure occurs between the neighboring plies, in the resin rich interface. Due to the low strength of the matrix, laminates generally have a poor interlaminar strength. The presence of significant out-of-plane (peeling) stresses can therefore cause interlaminar debonding fractures, also known as *delaminations*. Delaminations can also form as a result of voids or imperfections at the interface, intralaminar matrix crack joining or impact loading. Figure 8 shows a damage pattern caused by a low-velocity impact on a wing skin CFRP laminate of Gripen aircraft.

In FRP composites, in contrast to aluminum, delaminations can form from a relatively light impact, e.g. from a dropped tool. The delamination damage is hidden below the laminate surface and might remain undetected during visual inspections. Subsequent loading of the impact damaged structure might then lead to rapid delamination growth and a catastrophic failure of the laminate structure. Designing against this failure mode can be problematic, as it diminishes the influence of high strength of the fibers and instead lets the matrix properties govern the structural strength.

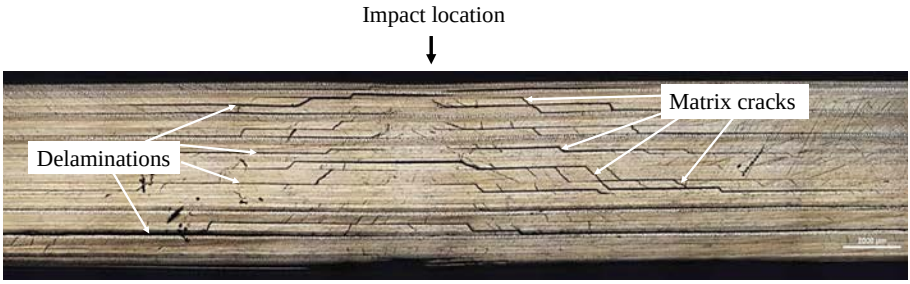

Figure 8: Low-velocity impact damage in the wing skin.

2.2 Fatigue damage development

Fatigue life of any cyclically loaded structure, independently of its material constitution, can be divided in three stages: crack (and/or damage) initiation, crack growth and final failure. In metals, the first stage is a consequence of irreversible movement of dislocations within the crystalline structure. These plastic deformations cause a cyclic slip process which leads to nucleation of micro-cracks at the free surface of the material. Initiation of fatigue damage can occur at stress levels well below the yield strength, and it often takes place at stress concentrations, e.g. holes, cut-outs, radii, inclusions, defects etc. Further cyclic loading promotes the increase of a micro-crack to a macro-crack, which is of order of a millimeter. Cracks of this size can be detected by current inspection methods and they signify the start of the second stage of fatigue life in metals. The existence of a macro-crack causes an increase in the local stress intensity, which generally accelerates the growth rate. Continued cycling extends the crack length further, until total fracture whereupon the static failure of the component occurs. Generally, the crack has a tendency to grow perpendicular to the loading direction. The three stages of fatigue life of metals are illustrated in Fig. 9.

Composite laminates exhibit a very different fatigue damage accumulation behavior. In the initiation stage, the damage onset on micro-scale is driven by the same mechanisms as in monotonic loading, i.e. matrix cracking, fiber fracture/kinking, fiber/matrix debonding and interlaminar cracking. However, the processes, cf. dislocation movement in metals, that lead up to formation of these micro-damages are not fully understood yet. The initiation of the fatigue damage starts at stress concentrations, preferably where significant out-of-plane stresses are present, i.e. holes, free edges, ply drop-off regions, impact damages etc. The second stage of the fatigue life is characterized by multiplication of micro-damages and formation and growth of one or several distinguishable delaminations. The delaminations are, in contrast to cracks in metal, oriented parallel to the main loading direction and are promoted by existence of out-of-plane stresses. For composites, the final stage of failure takes place by significant decrease of stiffness and loss of functionality. In components loaded in compression this could occur by buckling of the delaminated

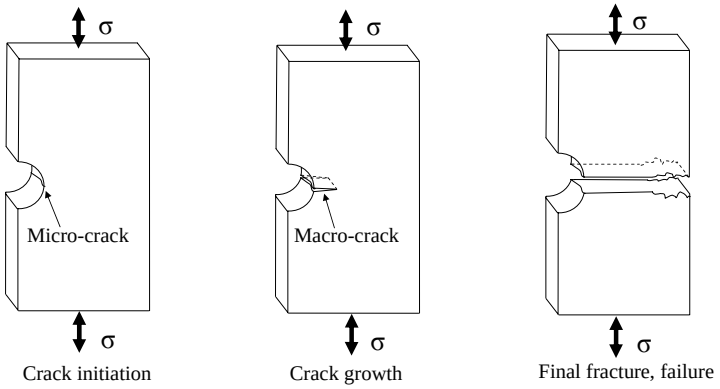

Figure 9: Initiation and growth of a fatigue crack to failure in a metal component.

plies. The fatigue damage progression of a composite laminate is shown in Fig. 10. Despite the efforts of the research community, the fatigue damage mechanisms in composite materials are, due to their complexity, yet not fully understood. This field remains an active area of research both from experimental and from modeling point of view.

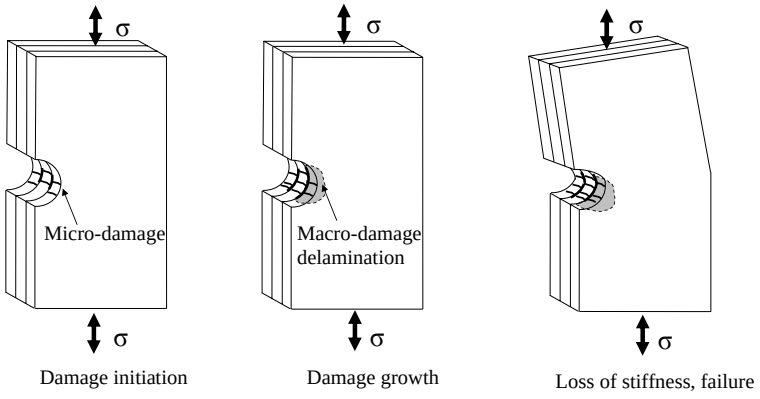

Figure 10: Initiation and growth of a fatigue damage in a composite laminate.

It is also worth mentioning that the composites generally have high stress concentration sensitivity in static loading. However, this sensitivity decreases with accumulation of fatigue damage as a result of gradual stiffness degradation. For aluminum, the case is exactly the opposite. This is illustrated in Fig. 11 in an S-N diagram.

The behavior of notched components has far-reaching consequences for design of both aluminum and CFRP components. Figure 11 shows that the notched CFRP

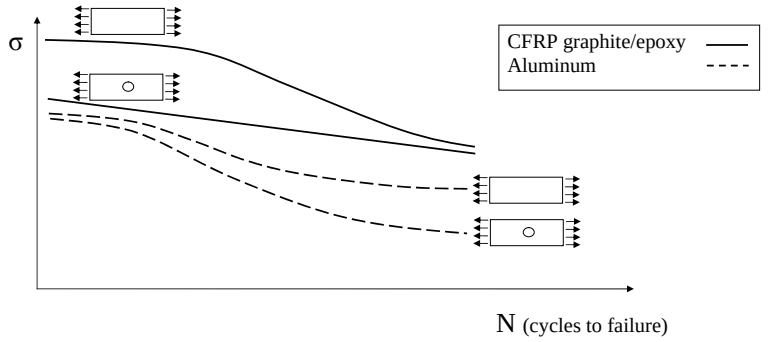

Figure 11: Comparison of typical S-N curves for CFRP and aluminum, notched and un-notched specimens.

curve has a low slope. If the CFRP component is designed so that the stress at N=1 is not exceeded at the maximal assumed static load, then the operational loads (fatigue loads) should cause stresses that are below the endurance limit. In other words, the ratio between the static strength and endurance limit is lower than the ratio between the maximal static load and the maximal operational load. This is the reason why composites are dimensioned considering static loading only. Aluminum, on the other hand, displays a considerable difference between the static strength and endurance limit, which is why fatigue has to be considered.

Similar situation arises when growth rates of cracks in aluminum and delaminations in CFRP are compared, see Fig. 12. For aluminum, the gap between the value of critical energy release rate and the threshold value is considerable, which is why stable crack growth can be allowed within the damage-tolerant approach. Also, if the component is dimensioned to withstand the maximal expected static load at the end of the crack growth, then the operational loads will give energy release rates that are above the threshold value. For delamination growth in composite, the span between the threshold value and the critical value is very small. This means that, if the laminate is sized so that the maximal expected static load gives the energy release rate that is below the critical value, then the operational loads will give the values which are below the threshold. Thus, the damage-tolerant approach for composites aims at designing the structure so that anticipated damages (delaminations) remain non-propagating during the service. This is known as the no-growth concept.

When strength and fatigue characteristics of materials are assessed with experiments, by an S-N curve or other data, scatter is always observed. The amount of scatter is quantified by statistical analysis methods and the results are considered in dimensioning and subsequent structural testing. In this way, the effect of material property scatter is incorporated in the structural design. Composite materials are believed to display a generally larger scatter than metals. This notion is based

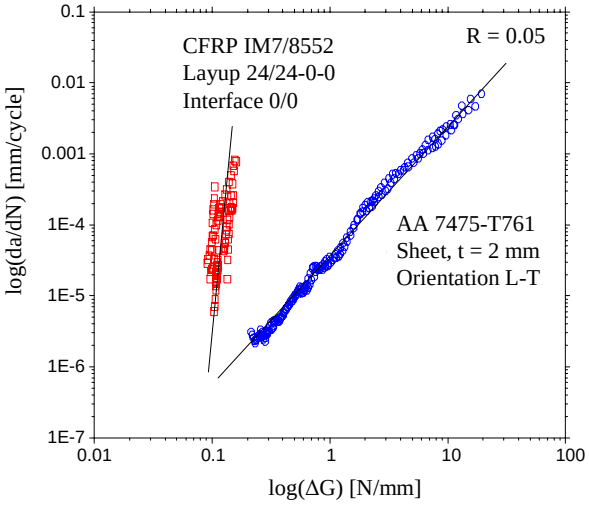

Figure 12: Comparison of crack/delamintaion growth rate da/dN as function of energy release rate ΔG for CFRP and aluminum.

on an investigation conducted in [20] and is today a topic of discussion. Several recent studies on composites display, according to [21], a scatter that is approaching that of metals.

Before concluding this chapter, one more difference between aluminum and composite behavior is highlighted. When exposed to variable amplitude and spectrum loading, metals tend to exhibit retardation in the crack growth rate subsequent to single tensile overloads [22]. This phenomenon is considered when design load spectra are defined for metal structures and high loads that cause crack growth retardation are usually excluded. In composites, no retardation effect is observed. On the contrary, it is the high spectrum loads that are the main cause of damage initiation and propagation.

The material differences presented in this chapter are the reason behind the different design methods, requirements and certification procedures for aluminum and CFRP aircraft components. The problem arises when hybrid structures, which seemingly have to comply with both of its constituents requirements at the same time, are considered. This is discussed in Paper 1 and in the next chapter.

3 Certification of aircraft structures

Certification of aircraft structure includes a large number of engineering aspects such as strength, durability, flutter etc., and covers the whole life span of the aircraft from concept to disposal. Certification of large civil aircraft is governed by international rules such as FAR25 [23] and military aircraft by specifications such as the US MIL-STD-1530 [24] and the UK Defence Standard [25]. The present work is focused on strength, stability, fatigue life and damage tolerance of hybrid structures and the following presentation regarding certification issues is limited to aspects that have bearing on these properties.

The aim of certification is to provide requirements and guidance for the design of aircraft to meet the airworthiness and customer requirements. The MIL-STD-1530 aims to ensure the structural integrity of an aircraft system through a number of time related tasks from initial design through the entire operational life of a fleet. Before the aircraft system enters the operational service, several tasks concerning design analyzes, development tests and full-scale verification tests are conducted, see Fig. 13. The last tasks are attributed to the preparation of data and procedures for safe operation of the fleet of aircraft during its service life and for the implementation of these measures.

3.1 Analysis

Based on the design information and mission analysis, an operational user profile is established and used as input to load analysis. Load analysis determines the magnitude and distribution of significant static and dynamic loads, which the aircraft structure may encounter when operated. This analysis consists of a determination of a variety of different loads and when applicable, the effects of temperature, aero-elasticity, and dynamic response of the aircraft structure. Design service loads spectra are developed to establish the distribution, frequency, and sequencing of loadings that the aircraft structure will experience based on the design service life and usage. Next, the structural analysis of the whole aircraft is performed in order to determine the load distribution.

In a strength, fatigue life and damage tolerance perspective, the stress analyzes and sizing of structural components are central issues. The stress analyzes include the analytical determination of the internal loads, stresses, strains, deformations which

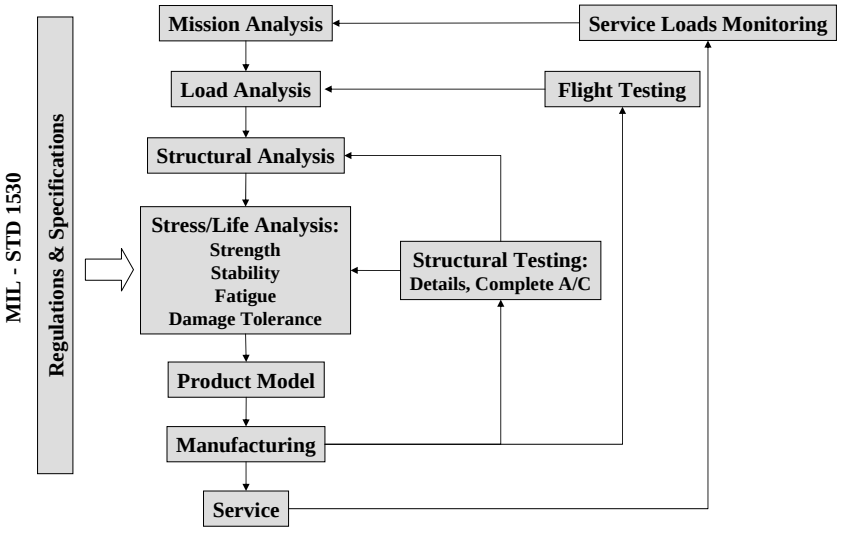

Figure 13: Aircraft structural integrity program.

result from the external loads and environments imposed on the aircraft structure. In the static strength analysis is it shown that the structure has sufficient strength so that it can carry *limit loads* without detrimental deformations, which would interfere with its safe operational and maintenance capabilities. The structure must be able to sustain *ultimate loads* without rupture or collapsing failure. In addition to verification of strength, the stress analysis is also used as a basis for stability, fatigue and damage-tolerance analyzes.

Damage tolerance analysis is conducted to substantiate the ability of the structural components to sustain cracks and defects safely until they are detected and maintained. A structure is considered to be damage tolerant if a maintenance program has been implemented that will result in the detection and repair of accidental damage, corrosion and fatigue cracking before such damage reduces the residual strength of the structure below an acceptable limit. The approach to account for damage tolerance is based on the assumption that defects can exist in any structure from the initial usage of the aircraft and that such defects can propagate with usage under fatigue loads. The design flight-by-flight stress/environment spectra are used in the damage growth analysis i.e. the computations of critical flaw sizes, residual strengths, safe damage growth periods and inspection intervals.

The above mentioned requirements are generally applicable to all material types but are implemented differently for composites than for aluminum, because of their dissimilar material behavior. The stress in aluminum components must be under

the failure stress at ultimate load and under the yield stress at limit load. Buckling of aluminum is allowed as long as the strength criteria are fulfilled. Damage tolerance is considered by assuming an initial crack which, under operational loading, can grow stably to a non-critical size whereupon the structure must be able to withstand the residual strength load.

Composite design allowables, for ultimate load, and reduction for environmental deterioration are set to approximately the same level as the fatigue endurance limit. This low level is assumed to cover the flaw tolerant aspect of the requirements as well, i.e. that the structure should sustain a certain amount of the undetected damage present. Currently, that amount is equivalent to a 6 mm hole present anywhere in the structure, which is a very rough estimate of a potential delamination damage induced by, for instance, impact. The difference of composites strength in tension and compression is not taken into account. Based on the limited stable delamination growth characteristics of the composites, cf. Fig. 12, no delamination growth is allowed. The low allowables also prevent the occurrence of buckling in the composite. Buckling of composite panels can induce peeling stresses and promote delaminations, which is why buckling is not allowed at any load level.

These conservative requirements for composites are reassessed in Paper 1 in the conceptual studies of the hybrid wing structure. The aim is to study the effect of alternative requirements on the structural weight, in the context of different hybrid designs exposed to thermo-mechanical loading. In the altered requirement set, buckling is allowed above a certain load level. The amount of sustainable damage and its corresponding allowable strain are determined from risk analysis and residual strength tests of impacted specimens. The resulting new allowables differ for compressive versus tensile loading and depend on where on the structure the damage occurs.

The conceptual studies also include a comparison of two different hybrid wing structural concepts by analysis. Figure 14 shows the spar cross-sections of the two concepts and an all-composite baseline design. The comparison considers the mass, structural behavior, strength, interaction between composite and aluminum, influence of thermal load and the significance of the altered requirements. Results from FE-analysis using the current requirements are shown in Fig. 18 and using the renewed requirements in Fig. 19. Based on these criteria concept 1 is chosen for further analysis and structural testing.

The assessment of composite structures by analysis and detailed modeling is a complex task. The difficulties arise as a result of the variability of the material behavior and failure modes described in Chapter 2. Typical engineering problems include: strength prediction in laminates, failure at fasteners and holes, delamination initiation and growth, impact, ply drop-off regions, fatigue damage accumulation, out-of-plane stresses etc. In order to assess the structural response in an accurate way, the modeling techniques suited for industrial usage need to be developed.

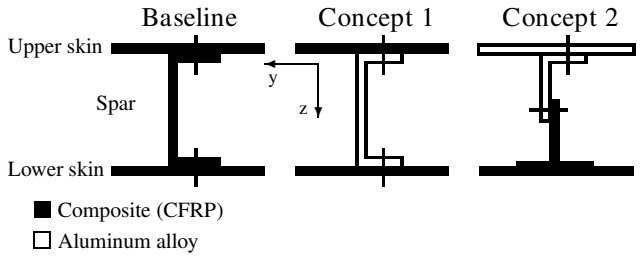

Figure 14: Cross-sections of the baseline design and the two hybrid concepts studied.

3.2 Testing

Test verification with full-scale assemblies of complete airframe is mandatory in aircraft certification requirements. Verification through testing is required for static strength, damage tolerance and fatigue life.

For a metallic structure it is not possible to use the same test article to demonstrate both static strength up to ultimate load conditions and fatigue life. The reason is that high static loads will introduce plastic deformation in positions of stress concentrations and leave beneficial residual stresses when unloaded, which can delay the initiation and growth of fatigue cracks. This is not acceptable since the test is intended to show the safe fatigue life of all aircraft of the type tested, also for those individuals who will not experience high loads during its operational life. It is well established to use safety factors on the design service life to show safe operational life for metallic structure. Factors between two and six have been used historically.

Composite structure on the other hand behaves differently since such structure is more susceptible for high loads which can initiate damages that may propagate under service loads. Composite strength is also more susceptible for heat and moisture content, which in most cases are impossible to impose on a full-scale test of a complete airframe. It is common to compensate the knock-down in static strength due to environmental influence by use of higher test loads than the design ultimate loads.

It is also required to show flaw tolerance for manufacturing discrepancies and service damages such as undetected impact damages for composite structure under operational loads. Also, the susceptibility for damage initiation and delaminations growth under operational loads at stress concentrations is of concern in a test verification perspective. There is an established knowledge that composites show a larger degree of variability in fatigue and damage growth properties [21]. Due to the higher variability in composites compared to metals, higher safety factors than those used for metals are required. An alternative approach has been applied in the aircraft industry in order to limit the long duration of testing time such factors

will result in. The approach makes use of a smaller safety factor on life which is compensated with an enlargement factor on loads. The factor on loads is known as the load enhancement factor (LEF) and results in a shorter test duration. The above differences between composite and metal structure highlight a wide variety of challenges when a hybrid metal/composite structure are to be verified by full-scale testing.

4 Constitutive modeling

This chapter presents and discusses existing material modeling techniques for laminated composites. The models discussed include elastic behavior, damage initiation and damage progression, and are suited for numerical implementation with FEM. Some of the models are utilized in this thesis work in a modified form and others are presented for the sake of overview. The framework for constitutive modeling of metals is well-established and is not treated in this work. Comprehensive descriptions can be found in [7]-[9] and the numerical implementation aspects are explained in detail in [26].

4.1 Elastic behavior

As mentioned before, single composite laminae are often modeled as homogeneous orthotropic entities. This means that the characteristics of lamina micro-structure, i.e. fibers, matrix and fiber/matrix interface, are disregarded. Instead, the lamina is idealized as a homogeneous continuum and assigned properties that are independent of position of the material point. Orthotropy, however, implies direction dependence of the properties. The linear elastic response of any material point within a lamina can then be described by *Hooke's generalized law*. The relation between the stress and the strain tensor then becomes

$$\sigma_{ij} = C_{ijkl}\epsilon_{kl} \quad \text{or} \quad \epsilon_{ij} = S_{ijkl}\sigma_{kl} \tag{4.1}$$

where C_{ijkl} and S_{ijkl} are fourth-order tensors known as the stiffness and compliance tensors, respectively. Both tensors have the so-called minor and major symmetry properties and are positive definite. The stress and strain tensors are also symmetric. If the coordinate axes are chosen as parallel to the material axes of orthotropy, i.e. 1, 2, 3 directions in Fig. 4, the second relation in Eq. (4.1) can be written in matrix form using Voigt notation in terms of engineering elastic constants as

$$\begin{bmatrix} \epsilon_{11} \\ \epsilon_{22} \\ \epsilon_{33} \\ 2\epsilon_{12} \\ 2\epsilon_{13} \\ 2\epsilon_{23} \end{bmatrix} = \begin{bmatrix} \frac{1}{E_1} & \frac{-\nu_{21}}{E_2} & \frac{-\nu_{31}}{E_3} & 0 & 0 & 0 \\ \frac{-\nu_{12}}{E_1} & \frac{1}{E_2} & \frac{-\nu_{32}}{E_3} & 0 & 0 & 0 \\ \frac{-\nu_{13}}{E_1} & \frac{-\nu_{23}}{E_2} & \frac{1}{E_3} & 0 & 0 & 0 \\ 0 & 0 & 0 & \frac{1}{G_{12}} & 0 & 0 \\ 0 & 0 & 0 & 0 & \frac{1}{G_{13}} & 0 \\ 0 & 0 & 0 & 0 & 0 & \frac{1}{G_{23}} \end{bmatrix} \begin{bmatrix} \sigma_{11} \\ \sigma_{22} \\ \sigma_{33} \\ \sigma_{12} \\ \sigma_{13} \\ \sigma_{23} \end{bmatrix} \tag{4.2}$$

where E_1, E_2, E_3 are Young's moduli in the principal material directions, ν_{ij}, $i \neq j$ are Poisson's ratios and G_{12}, G_{13}, G_{23} are shear moduli.

The thickness of a lamina is small compared to its other dimensions. Based on this, it can be assumed that a lamina, which is exposed to in-plane loading, is in state of plane stress, i.e. $\sigma_{33} = \sigma_{13} = \sigma_{23} = 0$. Consequently, Eq. (4.2) can be reduced to

$$\begin{bmatrix} \epsilon_{11} \\ \epsilon_{22} \\ 2\epsilon_{12} \end{bmatrix} = \begin{bmatrix} \frac{1}{E_1} & \frac{-\nu_{21}}{E_2} & 0 \\ \frac{-\nu_{12}}{E_1} & \frac{1}{E_2} & 0 \\ 0 & 0 & \frac{1}{G_{12}} \end{bmatrix} \begin{bmatrix} \sigma_{11} \\ \sigma_{22} \\ \sigma_{12} \end{bmatrix} \tag{4.3}$$

The stiffness relation is then found as

$$\begin{bmatrix} \sigma_{11} \\ \sigma_{22} \\ \sigma_{12} \end{bmatrix} = \frac{1}{1 - \nu_{12}\nu_{21}} \begin{bmatrix} E_1 & \nu_{21}E_2 & 0 \\ \nu_{12}E_1 & E_2 & 0 \\ 0 & 0 & (1 - \nu_{12}\nu_{21})G_{12} \end{bmatrix} \begin{bmatrix} \epsilon_{11} \\ \epsilon_{22} \\ 2\epsilon_{12} \end{bmatrix} \quad \text{or} \quad \bar{\boldsymbol{\sigma}} = \bar{\boldsymbol{Q}}\bar{\boldsymbol{\epsilon}} \tag{4.4}$$

where $\bar{\boldsymbol{\sigma}}$ is the stress matrix, $\bar{\boldsymbol{\epsilon}}$ is the strain matrix and $\bar{\boldsymbol{Q}}$ is the lamina stiffness matrix. The bars indicate that the matrix components are expressed in the local, lamina coordinate system, i.e. 1, 2, 3 directions in Fig. 4. The equations presented above are valid for single laminae but they can be used to construct a relation between the applied in-plane loads and strains in a stacked laminate. The solution, known as the *classical laminate plate theory* (CLPT) is very briefly summarized

here and the details can be found in [27]. This approach requires that the stacked laminae are of uniform thickness and that they are rigidly bonded to each other. Further, the laminate plate thickness is considered to be small in comparison to the other dimensions. Applying the Kirchhoff assumption, i.e. that the straight lines perpendicular to the midsurface of the plate remain straight, perpendicular and inextensible after the deformation, the laminate strain matrix can be written as

$$\boldsymbol{\epsilon} = \boldsymbol{\epsilon}_0 + z\boldsymbol{\kappa} \tag{4.5}$$

where $\boldsymbol{\epsilon} = [\epsilon_x \;\; \epsilon_y \;\; \gamma_{xy}]^T$ is the matrix containing the laminate strains expressed in the global coordinate system, $\boldsymbol{\epsilon}_0 = [\epsilon_{x0} \;\; \epsilon_{y0} \;\; \gamma_{xy0}]^T$ is matrix containing the strains of the middle surface expressed in the global coordinate system, $\boldsymbol{\kappa} = [\kappa_x \;\; \kappa_y \;\; \kappa_{xy}]^T$ is the curvature matrix and z is the coordinate in the thickness direction, measured from the middle surface. Now, defining the cross sectional distributed force and moment matrices as $\boldsymbol{N} = [N_x \;\; N_y \;\; N_{xy}]^T$ and $\boldsymbol{M} = [M_x \;\; M_y \;\; M_{xy}]^T$, and considering equilibrium between these and the lamina stresses across the cross section, the following is obtained

$$\begin{bmatrix} \boldsymbol{N} \\ \boldsymbol{M} \end{bmatrix} = \begin{bmatrix} \boldsymbol{A} & \boldsymbol{B} \\ \boldsymbol{B} & \boldsymbol{D} \end{bmatrix} \begin{bmatrix} \boldsymbol{\epsilon}_0 \\ \boldsymbol{\kappa} \end{bmatrix} \tag{4.6}$$

where the so-called $\boldsymbol{ABD}$-matrix is

$$\big[\boldsymbol{A}, \boldsymbol{B}, \boldsymbol{D}\big] = \sum_{k=1}^{n} \boldsymbol{Q}_k \left[(z_k - z_{k-1}), 1/2(z_k^2 - z_{k-1}^2), 1/3(z_k^3 - z_{k-1}^3)\right] \tag{4.7}$$

with $\boldsymbol{Q}_k = \boldsymbol{T}_k \bar{\boldsymbol{Q}}_k \boldsymbol{T}_k^T$ beeing the stiffness matrix of k^{th} lamina in the global coordinate system, $\bar{\boldsymbol{Q}}_k$ being the lamina stiffness matrix as defined in Eq. (4.4), z_k being the z-coordinate of the k^{th} lamina and $\boldsymbol{T}_k$ being the transformation matrix between the lamina stresses in local and global coordinate systems. Given the lamina properties, $\bar{\boldsymbol{Q}}$ can be constructed and with the laminate stacking sequence information, the $\boldsymbol{ABD}$-matrix can be obtained. For given set of forces and moments Eq. (4.6) can then be solved for $\boldsymbol{\epsilon}_0$ and $\boldsymbol{\kappa}$, which with Eq. (4.5) gives the strains over the laminate cross-section. Finally, these strains can be transformed into local coordinate strains using $\boldsymbol{T}$ and to local coordinate stresses using Eq. (4.4).

Both the lamina constitutive relation Eq. (4.2) and the laminate equation Eq. (4.6) are suitable for implementation in a FE-code. In the cases when each lamina is modeled individually with at least one element through the thickness, the inverse of

the compliance matrix in Eq. (4.2) enters the element stiffness matrix in a straight forward manner. If the whole laminate section, or parts of it, are modeled with one element through the thickness, the $\boldsymbol{ABD}$-matrix is used in the formulation of the element stiffness matrix. The summation in Eq. (4.7) is performed in the thickness direction over all layers within the element to obtain the $\boldsymbol{ABD}$-matrix. Once the element nodal displacement are solved, the strains and stresses in each layer are obtained in the same way as described above. In commercial FE-codes, elements that use this formulation are usually referred to as *layered elements* and they can be of different types, i.e. plane, plate, shell or solid elements. Regardless of how the boundary-value problem is solved, the obtained lamina stresses in each material point can be compared to the local failure criteria.

The non-linear shear stress-strain relationship mentioned in Chapter 2, is often represented by a third-order polynomial [28]

$$\gamma_{12} = \frac{1}{G_{12}}\tau_{12} + \alpha\tau_{12}^3 \tag{4.8}$$

where α is a curve fitting parameter that is determined experimentally.

4.2 Failure criteria

Individual plies within a laminate exhibit different local failure behavior based on the local stress state, as described in Chapter 2. Assuming linear elastic behavior, the stress and strain states can be obtained as functions of increasing applied load using the models in the previous section. In each individual lamina, intralaminar failure criteria can then be applied to determine the failure initiation point and maximal load-bearing capacity of the lamina. The failure criteria are commonly expressed in the form

$$f^m(\sigma_{ij}, \epsilon_{ij}, \bar{\sigma}_{ij}, \bar{\epsilon}_{ij}) = 1 \tag{4.9}$$

where $\bar{\sigma}_{ij}$ and $\bar{\epsilon}_{ij}$ symbolically denote the unidirectional laminate strengths and failure strains respectively and f^m denotes the failure function of mode m. A vast number of different failure criteria has been developed over the years and some of them are reviewed in [29]. An assessment and comparison of predictive capabilities of a large number of failure criteria was conducted in [30] in a World-Wide Failure Exercise (WWFE) and recommendations for designers were published. In this section, some of the most commonly used criteria, as well as criteria utilized in this work, are presented.

4.2.1 Limit criteria

The *maximum stress* and *maximum strain* criteria belong to this group of criteria. According to the maximum stress criterion, failure initiation occurs when any of the lamina stresses in the material principal directions reaches its respective strength. This is expressed as

$$\frac{\sigma_{11}}{X} = 1 \quad \text{where} \quad \begin{array}{ll} X = X_T & \text{if} \quad \sigma_{11} > 0 \\ X = -X_C & \text{if} \quad \sigma_{11} < 0 \end{array} \tag{4.10a}$$

$$\frac{\sigma_{22}}{Y} = 1 \quad \text{where} \quad \begin{array}{ll} Y = Y_T & \text{if} \quad \sigma_{22} > 0 \\ Y = -Y_C & \text{if} \quad \sigma_{22} < 0 \end{array} \tag{4.10b}$$

$$\frac{|\sigma_{12}|}{S_{12}} = 1 \tag{4.10c}$$

where X_T and X_C are unidirectional laminate tensile and compressive strength in fiber direction, Y_T and Y_C are unidirectional laminate tensile and compressive strength in transverse direction and S_{12} is lamina shear strength. The maximum strain criterion is identical to Eq. (4.10) provided that the stresses are replaced with strains and the strengths are replaced with lamina failure strains. It is evident that these criteria are based only on evaluation of the strength in the material principal directions, i.e. no interaction between the stress/strain components is considered.

4.2.2 Polynomial criteria

These criteria have their origin in von Mises yield criterion for metals, which states that the initial yield occurs when the deviatoric strain energy reaches a certain value. This condition can be expressed by a singe polynomial function cf. Eq. (4.9) that signifies an effective stress quantity. Hill [31] extended this criterion for ductile anisotropic materials which was then further modified for composites by Azzi and Tsai [32]. The resulting polynomial expression is referred to as the *Tsai-Hill criterion* and yields

$$\left(\frac{\sigma_{11}}{X}\right)^2 + \left(\frac{\sigma_{22}}{Y}\right)^2 + \left(\frac{\sigma_{12}}{S_{12}}\right)^2 - \frac{\sigma_{11}\sigma_{22}}{X^2} = 1 \quad \text{where} \quad \begin{array}{ll} X = X_T & \text{if} \quad \sigma_{11} > 0 \\ X = -X_C & \text{if} \quad \sigma_{11} < 0 \\ Y = Y_T & \text{if} \quad \sigma_{22} > 0 \\ Y = -Y_C & \text{if} \quad \sigma_{22} < 0 \end{array} \tag{4.11}$$

The criterion considers the interaction between the stress components as well as the difference in normal tensile and compressive strengths. A drawback is that one must keep track of the sign of the normal stress in order to insert the correct strength into the polynomial. However, the criterion is based on behavior of ductile metals and takes no account of heterogeneity and diversity of failure modes in composites. Based on the lack of physical relevance for composites, the Tsai-Hill criterion has received some criticism, for instance in [33].

Another, more general polynomial criterion, known as the *Tsai-Wu criterion* was proposed in [34] and states that failure initiation occurs when

$$\frac{\sigma_{11}^2}{X_T X_C} + \frac{\sigma_{22}^2}{Y_T Y_C} + \frac{\sigma_{12}^2}{S_{12}^2} - 2F_{12}\sigma_{11}\sigma_{22} + (\frac{1}{X_T} - \frac{1}{X_C})\sigma_{11} + (\frac{1}{Y_T} - \frac{1}{Y_C})\sigma_{22} = 1 \quad (4.12)$$

Besides the five already mentioned strength constants, the interaction material parameter F_{12}, which is obtained by a biaxial normal load test, is required. This criterion suffers from the same drawback as the former one, namely that it makes no distinction between the different failure modes in composites. Another drawback is that the these criteria are independent of a superimposed hydrostatic stress, which is typical for metals but not for composites. Both of the above criteria are derived as special cases of a general polynomial criterion which can be expressed as

$$f = F_{ij}\sigma_{ij} + F_{ij}\sigma_{ik}\sigma_{kj} + ... = 1 \quad (4.13)$$

where $i, j = 1, 2$ and F_{ij} are material parameters.

4.2.3 Physically based criteria

In [35], the author starts with the general polynomial criterion in Eq. (4.13) and considers two extreme cases of a composite laminate: one with infinitely stiff fibers (matrix-controlled failure) and one with fiber-controlled failure. In each case, several terms cancel, leading to two separate polynomial expressions: one fiber-controlled and one matrix-controlled. The conclusion is that, when the anisotropy is an order of magnitude or greater, the decomposition of the criterion into fiber and matrix failure modes is necessary. The same conclusion can be drawn from assessment of the physical failure process described in Chapter 2. This has motivated many researchers to derive criteria based on physical characteristics of failure. Although the criteria are classified as physically based, they are often stated as a mixture of limit and polynomial expressions where the different failure modes are separated. A widely used 2D physical criterion, known as the *Hashin criterion* was published in [36] and was later modified into a 3D form in [37]. This criterion

was originally intended for fatigue failure prediction but has also been used for the prediction of static failure. It yields

Tensile fiber failure ($\sigma_{11} > 0$)

$$\left(\frac{\sigma_{11}}{X_T}\right)^2 + \frac{1}{S_{12}^2}(\sigma_{12}^2 + \sigma_{13}^2) = 1 \tag{4.14a}$$

Compressive fiber failure ($\sigma_{11} < 0$)

$$-\frac{\sigma_{11}}{X_T} = 1 \tag{4.14b}$$

Tensile matrix failure ($\sigma_{22} + \sigma_{33} > 0$)

$$\frac{1}{Y_T^2}(\sigma_{22} + \sigma_{33})^2 + \frac{1}{S_{23}^2}(\sigma_{23}^2 - \sigma_{22}\sigma_{33}) + \frac{1}{S_{12}^2}(\sigma_{12}^2 + \sigma_{13}^2) = 1 \tag{4.14c}$$

Compressive matrix failure ($\sigma_{22} + \sigma_{33} < 0$)

$$\frac{1}{Y_C}\left[\left(\frac{Y_C}{S_{23}}\right)^2 - 1\right](\sigma_{22}+\sigma_{33}) + \frac{1}{4S_{23}^2}(\sigma_{22}+\sigma_{33})^2 + \frac{1}{S_{23}^2}(\sigma_{23}^2-\sigma_{22}\sigma_{33}) + \frac{1}{S_{12}^2}(\sigma_{12}^2+\sigma_{13}^2) = 1 \tag{4.14d}$$

In between the two Hashin publications, Yamada and Sun [38] proposed a criterion suited for the fiber controlled laminates, i.e. laminates which are not controlled by the transverse lamina strength Y. The criterion is similar to Eq. (4.11) if $\sigma_{22} = 0$ and yields

$$\left(\frac{\sigma_{11}}{X}\right)^2 + \left(\frac{\sigma_{12}}{S_{is}}\right)^2 = 1 \quad \text{where} \quad \begin{array}{lll} X = X_T & \text{if} & \sigma_{11} > 0 \\ X = -X_C & \text{if} & \sigma_{11} < 0 \end{array} \tag{4.15}$$

and where S_{is} is the in-situ lamina shear strength determined from measurement in cross-ply laminates. Based on this expression, Chang and Chang [39] and Chang and Lessard [40], developed another criterion, which includes shear non-linearity [28]. Further modifications, including the out-of-plane stresses were introduced by Olmedo and Santiuste [41] in the context of failure modeling of single-lap bolted joints. This criterion is included in Paper 2 of this thesis, where it was utilized in FE-modeling of bolted joint failure. It yields

Tensile fiber failure ($\sigma_{11} > 0$)

$$\sqrt{\left(\frac{\sigma_{11}}{X_T}\right)^2 + \frac{\frac{\tau_{12}^2}{2G_{12}} + \frac{3}{4}\alpha\tau_{12}^4}{\frac{S_{12}^2}{2G_{12}} + \frac{3}{4}\alpha S_{12}^4} + \frac{\frac{\tau_{13}^2}{2G_{13}} + \frac{3}{4}\alpha\tau_{13}^4}{\frac{S_{13}^2}{2G_{13}} + \frac{3}{4}\alpha S_{13}^4}} = 1 \tag{4.16a}$$

Compressive fiber failure ($\sigma_{11} < 0$)

$$-\frac{\sigma_{11}}{X_C} = 1 \tag{4.16b}$$

Matrix in-plane failure

$$\sqrt{\left(\frac{\sigma_{22}}{Y}\right)^2 + \frac{\frac{\tau_{12}^2}{2G_{12}} + \frac{3}{4}\alpha\tau_{12}^4}{\frac{S_{12}^2}{2G_{12}} + \frac{3}{4}\alpha S_{12}^4} + \frac{\frac{\tau_{23}^2}{2G_{23}} + \frac{3}{4}\alpha\tau_{23}^4}{\frac{S_{23}^2}{2G_{23}} + \frac{3}{4}\alpha S_{23}^4}} = 1 \quad \text{where} \quad \begin{array}{ll} Y = Y_T & \text{if} \quad \sigma_{22} > 0 \\ Y = -Y_C & \text{if} \quad \sigma_{22} < 0 \end{array} \tag{4.16c}$$

Matrix out-of-plane failure

$$\sqrt{\left(\frac{\sigma_{33}}{Z}\right)^2 + \frac{\frac{\tau_{13}^2}{2G_{13}} + \frac{3}{4}\alpha\tau_{13}^4}{\frac{S_{13}^2}{2G_{13}} + \frac{3}{4}\alpha S_{13}^4} + \frac{\frac{\tau_{23}^2}{2G_{23}} + \frac{3}{4}\alpha\tau_{23}^4}{\frac{S_{23}^2}{2G_{23}} + \frac{3}{4}\alpha S_{23}^4}} = 1 \quad \text{where} \quad \begin{array}{ll} Z = Z_T & \text{if} \quad \sigma_{33} > 0 \\ Z = -Z_C & \text{if} \quad \sigma_{33} < 0 \end{array} \tag{4.16d}$$

Fiber-matrix shearing failure ($\sigma_{11} < 0$)

$$\sqrt{\left(\frac{\sigma_{11}}{X_C}\right)^2 + \frac{\frac{\tau_{12}^2}{2G_{12}} + \frac{3}{4}\alpha\tau_{12}^4}{\frac{S_{12}^2}{2G_{12}} + \frac{3}{4}\alpha S_{12}^4} + \frac{\frac{\tau_{13}^2}{2G_{13}} + \frac{3}{4}\alpha\tau_{13}^4}{\frac{S_{13}^2}{2G_{13}} + \frac{3}{4}\alpha S_{13}^4}} = 1 \tag{4.16e}$$

where Z_T and Z_C are unidirectional laminate tensile and compressive strength in out-of-plane direction and α is the material parameter from Eq. (4.8). In Eq. (4.16a), the third term under the square root is due to the contribution from the out-of-plane shear stress to the fiber failure. If $\alpha = 0$, and the shear strength $S_{12} = S_{13}$, the criterion reduces to the tensile fiber mode criterion proposed by Hashin [37]. Originally, Chang and Chang [39] assumed that S_{12} used should be the in-situ ply shear strength measured from a cross-ply laminate, since that value may differ significantly from the strength measured from unidirectional plies. Matrix out-of-plane failure is considered by expanding the Hashin [37] criterion for delamination initiation with the non-linear shear stress/strain behavior. The Hashin criterion Eq. (4.14) was also implemented in the context of bolted joint failure in Paper 2 and it was found that the results were very close to those obtained with the criterion in Eq. (4.16).

The intralaminar criteria presented above are based on the distinction of the fiber and matrix dominated failure. However, the resulting quadratic polynomial expressions are derived from phenomenological assumptions of stress interaction and

not on physical characteristics of failure. More elaborated models were proposed by Puck and Schürmann in [18] and [15], where attention was payed to critical planes where matrix cracks develop and interaction between the fibers and the matrix. Further development of Puck's criterion was performed by Davila et al. in [42] involving critical planes for matrix cracks, determination of in-situ strength using fracture mechanics and fiber-matrix interaction in development of kinking. A 3D version of this criterion including shear non-linearity was developed in [43].

In [29], a summary of interlaminar criteria for delamination initiation is presented. These models are similar to the quadratic polynomial intralaminar criteria previously presented. However, the interface failure initiation and progression is often modeled with FEM by introducing interfacial elements between the plies. A summary of available models is included in [29].

4.3 Damage progression

Once the state in a material point within a lamina, or between the laminae, has met a failure criterion, its load carrying capacity will decrease with further loading. Damage progression, signified by loss of the stiffness, will take place until the amount of dissipated energy has reached a critical value, whereupon final failure occurs. In a laminate, where the plies are exposed to different stress states, the failure of all plies will not occur simultaneously. Instead, when one ply has failed (first-ply failure (FPF)), redistribution of the load to the other plies will take place, which then may fail themselves. As the applied load is increased, the progression of failure and damage takes place. The ultimate strength of a laminate is reached when the load can not be further increased, i.e. last-ply failure (LPF).

A common modeling approach is to reduce the relevant terms of the lamina stiffness matrix depending on the failure mode. This is known as the *ply-discount method*, and it is used in this work in the context of bolt joint failure. The stiffness terms to be reduced are chosen by micro-mechanical considerations but the level to which they are reduced is somewhat arbitrary. The simplest alternative is to reduce all terms to zero as soon as the failure criterion is met. Such degradation corresponds to a sudden brittle failure with no energy dissipation in the damage process. This is not a very realistic assumption, since it has been confirmed in many experimental studies that the stress degrades gradually after the onset of failure. In their work, Zang and Rowland [44] and Tserpes et al. [45] concluded that the reduction of the stiffness matrix terms to zero gives a too severe degradation when compared to experimental results. It also causes convergence problems in the FE-modeling of bolts because the elements in the area of large contact pressure tend to become highly distorted. A more realistic set of degradation factors were introduced by Tan [46] and extended by Camanho [47] to three dimensions. Similar factors were used in [41], [44], [45], [48] all with good correlation to experimental results. The same degradation factors are used in this work and are shown in Table 1.

Failure mode	E_{11}	E_{22}	E_{33}	G_{12}	G_{13}	G_{23}	ν_{12}	ν_{13}	ν_{23}
Matrix failure	-	0.4	0.4	-	-	0.2	0	0	0
Fiber failue	0.14	0.4	0.4	0.25	0.25	0.2	0	0	0
Fiber-matrix shear	-	-	-	0.25	0.25	-	0	0	-

Table 1: Degradation rules in different failure modes.

Alternative approaches to modeling damage and subsequent loss of stiffness in composite materials have been developed in the context of continuum damage mechanics (CDM). After the failure criterion is met, the damage development due to each failure mechanism is typically controlled by a damage variable. The material stiffness properties are successively reduced depending on the current damage state, which in turn depends on a chosen damage evolution law. This law is thus a key parameter in the framework of CDM. The choice of law is often based on some kind of physical or energy-conserving ground. Usually, the damage variable has a value of 0 at failure initiation and increases to 1 during the damage accumulation whereafter the material stiffness is considered exhausted. A large number of CDM-models are published in the literature and some examples are found in [16], [49], [50]-[53]. The typical framework is based on the second law of thermodynamics, which is expressed through the Clausius-Duhem inequality [7]. Under relevant conditions this can be written as

$$\left(\frac{\partial G}{\partial \sigma_{ij}} - \epsilon_{ij}\right)\dot{\sigma}_{ij} + \frac{\partial G}{\partial d_m}\dot{d}_m \geq 0 \tag{4.17}$$

where $G = G(\sigma_{ij}, d_m)$ is Gibbs free energy and d_m is the damage variable of mode m. Since the stress tensor can be chosen arbitrary, the expression in the parenthesis must be equal to zero which with Eq. (4.1) leads to

$$\epsilon_{ij} = \frac{\partial G}{\partial \sigma_{ij}} = S_{ijkl}\sigma_{kl} \qquad \text{and} \qquad \frac{\partial G}{\partial d_m}\dot{d}_m \geq 0 \tag{4.18}$$

The first expression implies that the compliance tensor depends on the damage variables. Thus, as the damage accumulates during the failure process, the compliance changes. The inequality signifies that the energy dissipation due to the change of damage state cannot be negative. Once Gibbs free energy has been chosen so that the thermo-dynamic forces $\partial G/\partial d_m$ are positive, the sufficient condition for fulfillment of the second law is that the damage variables are non-decreasing functions. Apart from being non-decreasing, the damage functions are specified by a damage evolution law that is often determined from phenomenological or energy-conserving considerations. The notion of damage is, in classical sense of continuum damage mechanics, coupled to the loss of stress transmitting area. The remaining undamaged area is then subjected to effective stress $\widehat{\sigma}_{ij}$, which is related to the

strain through the undamaged compliance tensor S^0_{ijkl}, i.e. the compliance tensor for $d_m = 0$, as

$$\epsilon_{ij} = S^0_{ijkl}\widehat{\sigma}_{kl} \tag{4.19}$$

The effetive stress is related to the nominal stress σ_{ij} by introducting a damage operator M_{ijkl}

$$\widehat{\sigma}_{ij} = M_{ijkl}\sigma_{kl} \tag{4.20}$$

Combining Eq. (4.19) and (4.20) gives the stress-strain relation

$$\epsilon_{ij} = S^0_{ijkl}M_{klmn}\sigma_{mn} \tag{4.21}$$

which, when compared to Eq. (4.18) gives the compliance tensor $S_{ijmn} = S^0_{ijkl}M_{klmn}$.

The damage dependence of the compliance tensor is thus entirely controlled by the damage operator M_{ijkl}. The relation in Eq. (4.21) has a corresponding inverse relation, where the stiffness tensor depends on the damage variables. When implemented, the components of the damage operator are chosen to represent different types of damage, for instance fiber, matrix and shear damage. An example of such damage operator, using the Voigt notation, can be found in [51]

$$\boldsymbol{M} = \begin{bmatrix} \dfrac{1}{1-d_f} & 0 & 0 \\ 0 & \dfrac{1}{1-d_m} & 0 \\ 0 & 0 & \dfrac{1}{1-d_s} \end{bmatrix} \tag{4.22}$$

where d_f, d_m and d_s are fiber, matrix and shear damage variables.

The implementation of CDM-models in the FE-code can differ depending on the solution algorithm. If an explicit time integration algorithm is used, the global stiffness matrix is not computed. Instead the internal force vector is formed directly by integration of the stresses, thus including the effects of damage. If the Newton-Raphson algorithm is used to solve the non-linear equilibrium equations, the global stiffness matrix needs to be computed and inverted. For this purpose, the Jacobian matrix is computed as

$$\frac{\partial \boldsymbol{\sigma}}{\partial \boldsymbol{\epsilon}} = \boldsymbol{C} + \sum_m \frac{\partial \boldsymbol{C}}{\partial d_m} \frac{\partial d_m}{\partial \boldsymbol{\epsilon}} \tag{4.23}$$

where $\boldsymbol{C}$ is the damaged stiffness tensor.

The implemented material models are often demonstrated on regular coupons or specimens with open hole tension or compression and they often seem to work well. Bearing failure of bolted joints, on the other hand, is problematic in the sense that the area of damage concentration is also the area of contact between the bolt and the hole edge. A complete degradation of stiffness and the subsequent element deletion in the area of contact creates convergence problems and yields poor results. From a physical point of view and based on the experimental observations, material removal is unrealistic. The material that has failed due to the bearing failure mode seem to have some residual stiffness left but there is no obvious way to model this kind of behavior and further research is required.

5 Finite element modeling

In this chapter, the FE techniques used in this work are outlined. All simulations are preformed with the commercial FE-program Abaqus [54]. Theoretical details and implementation technique background can be found in [26], [55], [56] and composite specific topics in [57], [58]. Two types of models are developed in this work: global shell models of the hybrid wing box structure and local solid models of bolted hybrid joints.

5.1 Modeling of bolted joints

In the appended Paper 2, the detailed modeling of a single shear lap, composite-aluminum joint with countersunk titanium fastener is performed. A large number of studies of bolted joints with composite plates can be found in the literature [59]. They range from two-dimensional models with rigid pins representing the bolt [48], [60], [61], to three-dimensional models with or without damage development in the composite [41], [44], [47], [58], [62]-[68]. These studies include parameters as bolt pretension, bolt clearance, the effect of countersunk/protruding bolt heads, different failure initiation and damage progression models, by-pass loading, implicit/explicit solution methods etc. In the current work, this accumulated knowledge is utilized to develop local detailed models of hybrid fastener installations in the wing box. The response, in terms of a force-displacement curve, of a local model is then assigned to line elements representing the fasteners in a global model of the wing box. This is described in the next section. Before modeling the actual joint geometries in the wing box, the modeling method is first applied to a joint specimen of similar constitution, which has been tested in [69]. Figure 15 shows the mesh and the applied loading.

Each ply in the CFRP plate is represented with one solid element in the thickness direction, see Fig. 16, while the aluminum plate is assigned a somewhat lower solid mesh density. Aluminum and titanium materials are assigned elasto-plastic models with isotropic hardening. The normal stress-strain behavior in the composite plate is modeled as linear orthotropic, cf. Eq. (4.2), up to failure and for the shear stress-strain relation, Eq. (4.8) is used. In order to implement Eq. (4.8) into the FE-model, the non-linear term is rewritten such that a numerically stable algorithm

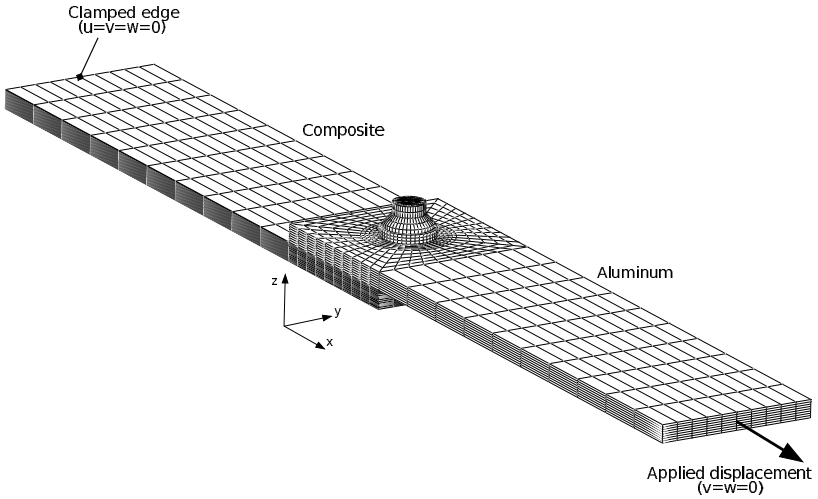

Figure 15: FE-model of a single-bolted hybrid joint specimen.

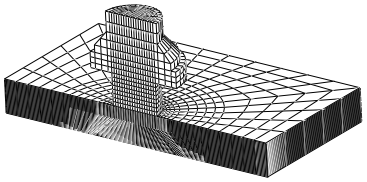

Figure 16: Close-up view of the mesh in the composite plate around the fastener.

is obtained, as described in [54]. The shear stress at the end of the load increment i is then given as a linear function of the shear strain

$$\tau_{12}^{(i+1)} = (1-d)G_{12}\gamma_{12}^{(i+1)} \tag{5.1}$$

where

$$d = \frac{3\alpha G_{12}(\tau_{12}^{(i)})^2 - 2\alpha(\tau_{12}^{(i)})^3/\gamma_{12}^{(i)}}{1 + 3\alpha G_{12}(\tau_{12}^{(i)})^2} \tag{5.2}$$

The parameter d can be seen as a damage parameter that degrades the initial shear modulus G_{12} to its current value $(1-d)G_{12}$.

The failure criterion employed is written in Eq. (4.16). After failure initiation, the material degradation is achieved with a ply-discount method by reduction of

relevant stiffness parameters. The degradation factors used were established in [46] and [47]. The material model is implemented into Abaqus as a user-defined subroutine, which is called by the solver in each increment. Further details about the failure criterion and degradation factors can be found in Paper 2. The model also includes a contact formulation with Coulomb friction for all relevant surfaces, with frictional coefficients from [70]. The solution is obtained by a standard Newton-Raphson algorithm. In Fig. 17, the applied force-displacement curve obtained by experiments in [69] is compared to curves resulting from the simulations. Three different simulations are considered, one without composite damage and without metal plasticity, one with metal plasticity but without composite damage, and one with both. The effect of including composite damage in the simulation is apparent from this comparison.

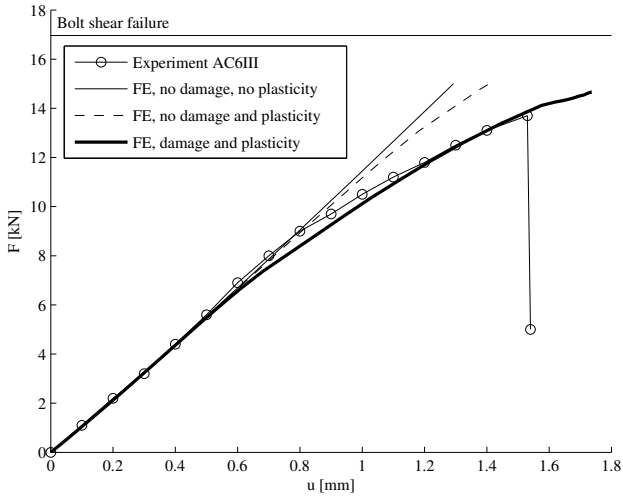

Figure 17: Comparison of the applied force-displacement curves obtained by experiments in [69] and results from simulations.

The current version of Abaqus does contain a progressive damage model for composite materials. It is based on CDM concept described in the previous chapter and uses the Hashin criterion to evaluate the initial failure. However, it is two-dimensional and not implemented for solid elements. In this work, an attempt was made to run a fastener model using continuum shell elements with the Abaqus progressive damage model for the composite plate. The kinematic and constitutive formulations for continuum shell elements [71] are identical to the conventional shell elements but their geometry is based on the three-dimensional solid description. Since these elements use reduced integration, it turned out that hourglass modes were triggered over large part of the contact area and the solution was destroyed. The results obtained with the ply-discount method captured the experimentally

observed behavior of the specimen well. The predicted damage initiation point concurred with the one obtained in testing, while the joint failure point was somewhat over-predicted. In the local models of the joints within the wing box, the predicted failure load was the same as the design failure load of the fastener in all cases.

5.2 Structural modeling

In both appended papers, FE-models of the wing-like structure in Fig. 3 are developed. The difference is that the structure in the conceptual studies consists of only one box, i.e. the splice section is not included, and that several types of cross-sections are considered. Also, in the conceptual studies, only pure bending and twisting loads are applied.

The focus in the conceptual study models is the middle section of the wing box, i.e. the area between the ribs. The remaining parts of the structure are included only to capture the effects of thermally induced stresses. All parts of the structure are modeled as their mid-surfaces with conventional shell elements in order to increase the computational efficiency. For the composite plates, the layered formulation without progressive damage is used, cf. Chapter 4. Only the initial failure is considered, by means of the maximum strain and Tsai-Hill criteria. Fasteners are represented using Abaqus *connector elements*, from which the fastener loads are extracted. These are two-node elements that impose a user-defined constraint between the nodes. The implementation is based on the use of Lagrange multiplier technique [56]. In the FE-models of the conceptual study, the fasteners are assigned a linear elastic stiffness without any damage behavior, and are only used to compute the transferred fastener load. Evaluation of static and fatigue failure is then handled by external programs. Contact conditions are modeled between all structural parts using a penalty contact formulation. All models are solved using a large displacement formulation and the Newton-Raphson algorithm. Figure 18 shows the resulting stress in the middle sections of two models from the conceptual studies. The figure illustrates the different structural behavior of the concepts. According to the current requirements, only aluminum components are allowed to buckle prior to the ultimate load level. It is also shown that the 90°C case is the worst case scenario for concept 1 and -30°C for concept 2. This is a result of the buckling requirement on this structural configuration. Figure 19 shows the resulting deformations within the frame of renewed requirements, where buckling is allowed for all components and temperature requirement is modified. It is worth mentioning that, in this case, the worst case thermal load is the same for both concepts.

The cross-section of the wing box chosen for the testing is of concept 2 type, with spars, ribs and splice of aluminum bolted to skins made of composite. The purpose of the structural modeling of the wing box in Paper 2 is to simulate the conditions

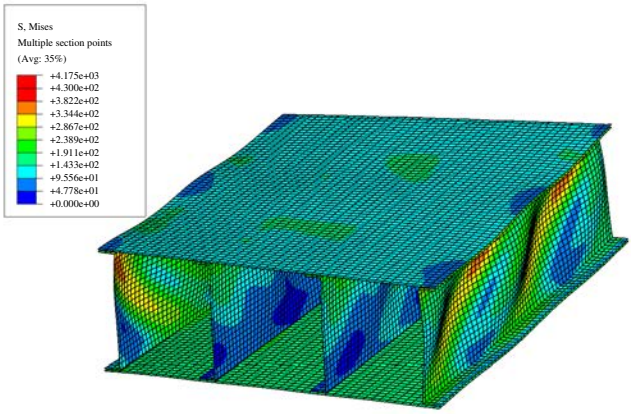

(a) Concept 1, at 90°C

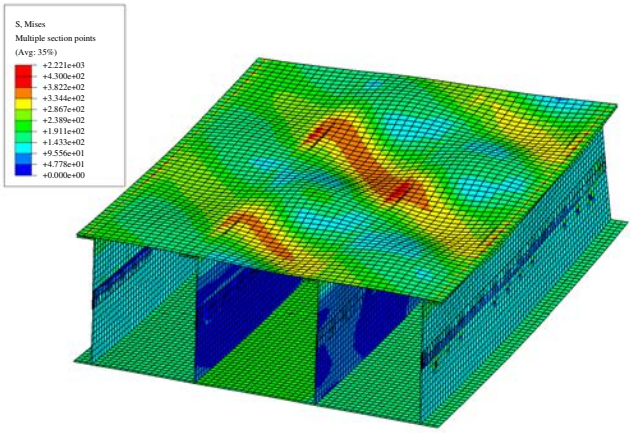

(b) Concept 2, at -50°C

Figure 18: Buckling pattern of the middle sections of the two studied hybrid concepts, ultimate bending/twisting load and applied temperature, current requirements.

in the testing and to include the local composite damage and metal plasticity in the fasteners. Several authors have developed methods to introduce non-linear fastener behavior in structural models. For example, Weyer et al. [72] used connector elements available in the Abaqus to represent self-piercing rivets in an explicit crash analysis. The modeling included elastic, plastic and damage behavior of a single bolted metal sheet specimen. Gray and McCarhty [73] developed a method using beam elements connected to a rigid surface to represent the bolt, and shell elements to model the laminate plates of the joint. Bolt-hole clearance, bolt-torque and friction between the plates were considered, but the damage dissipation in laminates was not accounted for. The functionality of the model was demonstrated

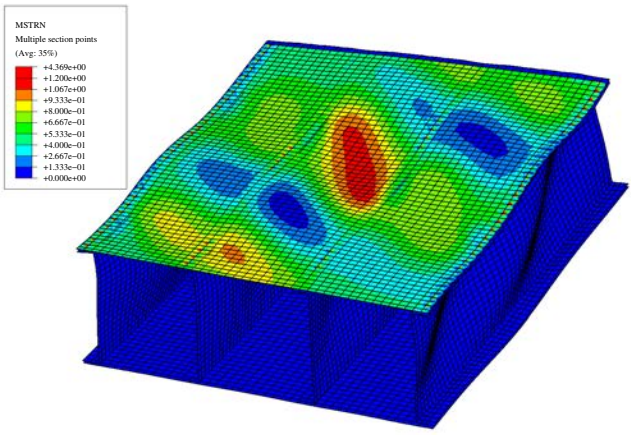

(a) Concept 1, at -30°C

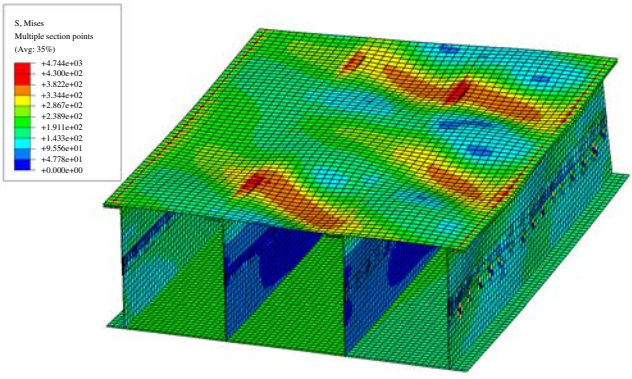

(b) Concept 2, at -30°C

Figure 19: Buckling pattern of the middle sections of the two studied hybrid concepts, ultimate bending/twisting load and applied temperature, new requirements.

on a three-bolt single-lap joint. Another efficient approach was developed by Gray and McCarthy [74], were a user-defined element was implemented in Abaqus. The method is capable of modeling non-linear behavior and failure of composite joints based on a semi-empirical approach. A joint with twenty fasteners was used for validation of the method. Ekh and Schön [75] made use of beam elements to represent both bolt and laminates, and connector elements to account for bolt-hole clearance and friction. The model was suited for optimization of load transfer, but was limited to single-column joints. A two-dimensional model of a steel-concrete beam with spring elements representing the shear connections was developed by Wang and Chung [76]. A non-linear behavior of the springs, based on experimental data was utilized.

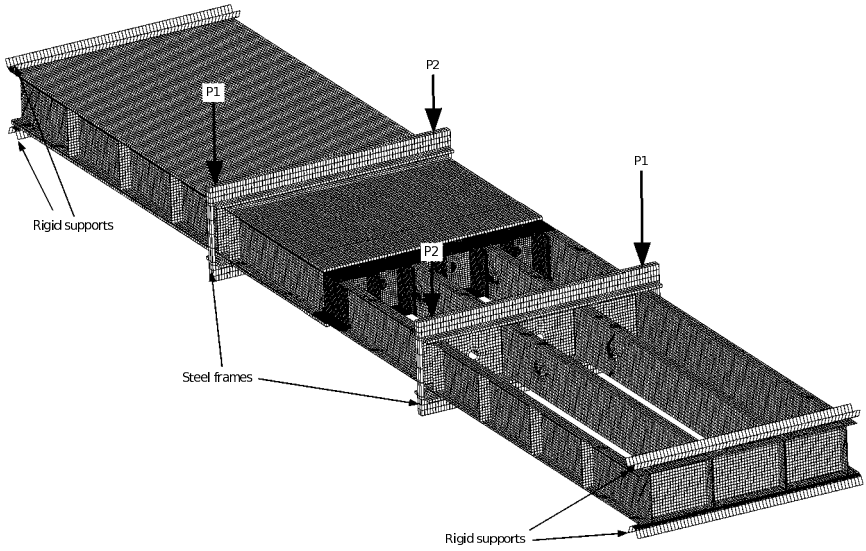

Figure 20: FE-model of the wing box structure.

In the test set-up, the wing box is supported at its ends on both upper and lower sides, while the mechanical loads are applied by four actuators via two steel frames clamped around the circumference of the box, as shown in Fig. 20. By applying the same load on the diagonally placed actuators, a proportional bending/twisting loading is achieved in the middle area. For modeling of aluminum parts, conventional shell element are used. Composite skins are modeled with continuum shell elements and for steel frames solid elements are used. Contact conditions are assigned between all parts in the structure. The wing box contains a large number of fasteners that connect the structural parts. The fasteners are modeled with two-node connector elements placed at the center axis of each fastener. An Abaqus built in feature is used to connect the structural parts with connectors independently of the mesh. This is achieved by placing multiple point constraints between the connector element nodes and the nodes of the connected parts. The behavior of the connectors is assigned to the elements as the force-displacement characteristics of the in-plane resultant fastener force. These characteristics are derived from local detailed models and they differ depending on the joint configuration. However, they all look principally the same as the curve in Fig. 17. After the maximal fastener shear load is reached, the force is ramped down to zero over a very small displacement range using the connector damage capability in Abaqus. Once a failure of a single fastener has occurred, the element is removed from the analysis and the load is redistributed to the other fasteners.

In the first step of the simulation, pretension forces are applied to the vertical braces of the steel frames. This pretension simulates the conditions in the testing,

where bolts are pre-torqued in order to hold the steel frame in position while the actuator loads are applied. In a subsequent step, a constant temperature of 70°C is applied to the entire box. In the final step, the actuator forces are applied as linearly increasing functions of the step time. At some point, the first fastener failure occurs and load redistribution takes place. After that, the process progresses by failure of the neighboring fasteners. The sudden loss of load carrying capacity in the fasteners creates local instabilities which in turn cause convergence difficulties in the solution process. The problem is handled by introduction of artificial stabilizing measures and local viscous damping. Figure 21 shows the redistribution of the fastener loads due to the progressive fastener failure in the splice section bolt rows.

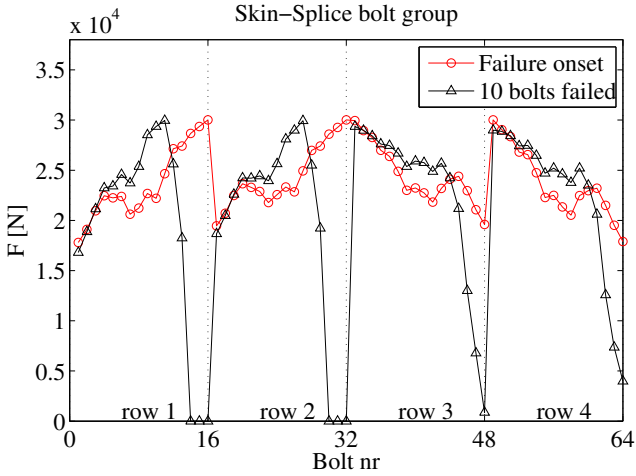

Figure 21: Progressive fastener failure in the splice section.

6 Outlook

In this work, the focus is directed on the strength analyzes and modeling of a hybrid structure. The main concerns are the interaction of composite and aluminum parts and the different structural requirements they may comply to, and the detailed modeling of the fastener installations. The modeling work is closely related to the ongoing testing of the wing box structure described in this thesis. The next step of the research effort is to evaluate the test results and to evaluate and compare the outcome of the results from the analytical predictions. The emphasis is put on the thermo-mechanical behavior, strength, stability, fatigue and damage tolerance characteristics.

In the analyzes, increased temperature resulted in a biaxial stress state in the fastener joints. It is unclear how this stress state affects the strength and fatigue life of the hybrid joints and experimental investigations are currently conducted on coupon test specimens to gain more knowledge. There is a possibility that the composite is affected in a totally different way than aluminum is. Further development of modeling techniques, which include softening of the composite material in fatigue loading, is needed in order to capture the conditions in the test. The testing on coupons is also intended to provide information about the scatter difference of aluminum and composite in fatigue, which may give increased knowledge to revise load enhancement factors for structural testing. Both constant amplitude and spectrum loading are included in the coupon testing. The effects of elimination of insignificant load levels in the spectrum and truncation of overloads for composite, aluminum and the hybrid will be studied.

The wing box structure contains an impact damage and artificial delaminations in the ply drop-off regions in the composite skin. Modeling work is currently conducted with the aim to simulate the impact event and subsequent loading in the structure. Interlaminar and intralaminar damage are considered using continuum damage models and cohesive elements. The artificial delaminations are modeled using virtual crack closure technique.

The structural testing of the wing box conducted in this research is substantially different from the typical structural verification testing. The test of the wing box is performed in order to assess the thermo-mechanical behavior of the hybrid structure and to find the critical features from static, fatigue and damage tolerant points of view. In the verification testing, the purpose is to evaluate whether or

not a representative structure complies with the requirements under the prescribed terms of use. The inherent variability of both material properties and load spectra need to be taken into account. This poses a problem for hybrid structures because of the mismatch of the variability between composite and aluminum. More research on the scatter in critical composite structural features needs to be done in order to establish more viable procedures for verification testing of hybrid structures.

7 Review of included papers

Paper I

Conceptual studies of a composite-aluminum hybrid wing box demonstrator

This work presents a conceptual study of two different cross-section designs of a hybrid wing box structure. The structure is designed given the thermal and mechanical loads and with respect to requirements, for static strength, fatigue and stability, currently used in the aircraft industry. The overall structural response is evaluated, as well as the local and structural failure modes. The resulting masses of the two concepts, subject to current requirements, are compared. Further, the requirements concerning allowable strains, allowable buckling load and given thermal loads are modified and another comparison is preformed. This comparison is performed between the two concepts, but also between the two different requirement set and their impact on the final masses of the concepts. Finally, one of the concepts is chosen to be used in design of a test.

Paper II

Finite element modeling of mechanically fastened composite-aluminum joints in aircraft structures

Mechanically fastened joints are widely used in structural design of aircraft. Due to the large number of fasteners in the structure, detailed FE-modeling of the structure including joints tends to be computationally expensive. In this paper, a methodology is developed in which the local hybrid joint behavior, including damage accumulation in composite and metal plasticity, is assessed first. This behavior, including fastener failure, is then assigned to structural elements representing the bolts in a global structural model. This technique is applied to a hybrid composite-aluminum wing box structure exposed to thermal and mechanical loading. An FE-model of the wing box in the test setup is developed and the

progressive failure of bolted joints is studied. The initial joint stiffness predicted with the local models agrees well with the semi-empirical stiffness commonly used in the industry today. At higher loads, however, due to damage development in the composite and aluminum plasticity, the force-displacement curve deflects from the linear. Simulations show that the fastener load distribution at high load levels is affected by this and that linear fastener models produce inaccurate results. It was also shown that the thermally induced loads give a significant contribution to the mechanical loads at considered temperatures.

Bibliography

[1] M. C. Y. Niu. Airframe structural design. Hong Kong Conmilit Press, Second edition, Hong Kong, 1999.

[2] R. S. Whitehead. Lessons learned for composite structures. The first NASA advanced composites technology conference, Part I, 399-415, Seattle, 1990.

[3] MIL-HDBK-17-3F. Military handbook, polymer matrix composites. U.S. Department of Defense, 2000.

[4] J. Rouchon. Certification of large airplane composite structures - recent progress and new trends in compliance philosophy. In 17^{th} ICAS Congress, Stockholm, 1990.

[5] R. Talreja and C. V. Singh. Damage and failure of composite materials. Cambridge University Press, Cambridge, 2012.

[6] MMPDS-04. Metallic materials properties development and standardization (MMPDS). Federal Aviation Administration, 2006.

[7] N. S. Ottosen and M. Ristinmaa. The mechanics of constitutive modeling. Elsevier, Oxford, 2005.

[8] J. Lemaitre and J. L. Chaboche. Mechanics of solid materials. Cambridge University Press, Cambridge, 1994.

[9] J. Lubliner. Plasticity theory. Macmillan, New York, 1990.

[10] V. V. Vasiliev and E. V. Morozov. Mechanics and analysis of composite materials. Elsevier Science, First edition, Oxford, 2001.

[11] I. M. Daniel and O. Ishai. Engineering mechanics of composite materials. Oxford University Press, Oxford, 1994.

[12] R. M. Jones. Mechanics of composite materials. McGraw Hill, New York, 1975.

[13] J. M. Hodgkinson. Mechanical testing of advanced fibre composites. Woodhead Publishing, First edition, Cambridge, 2000.

[14] A. K. Kaw. Mechanics of composite materials. CRC Press, Second edition, Boca Raton, 2006.

[15] A. Puck and H. Schürmann. Failure analysis of frp laminates by means of physically based phenomenological models. Composites Science and Technology, 62(12-13):1633–1662, 2002.

[16] A. Matzenmiller, J. Lubliner, and R. L. Taylor. A constitutive model for anisotropic damage in fiber-composites. Mechanics of Materials, 20(2):125–152, 1995.

[17] D. Hull and T. W. Clyne. An introduction to composite materials. Cambridge University Press, Second edition, Cambridge, 1996.

[18] A. Puck and H. Schürmann. Failure analysis of frp laminates by means of physically based phenomenological models. Composites Science and Technology, 58(7):1045–1067, 1998.

[19] P. P. Camanho, C. G. Davila, S. T. Pinho, L. Iannucci, and P. Robinson. Prediction of in situ strengths and matrix cracking in composites under transverse tension and in-plane shear. Composites Part A: Applied Science and Manufacturing, 37(2):165–176, 2006.

[20] R. S. Whitehead, H. P. Kan, R. Cordero, and E. S. Saether. Certification testing methodology for composite structure, Volume I: Data analysis and Volume II: Methodology development. Northrop Corporation, Hawthorne, 1986.

[21] J. Rouchon. Fatigue and damage tolerance evaluation of structures: The composite materials response. In 22^{th} Plantema memorial lecture, 25^{th} ICAF symposium, Rotterdam, 2009.

[22] S. Suresh. Fatigue of materials. Cambridge University Press, Second edition, Cambridge, 1998.

[23] FAR 25. Airworthiness Standards: Transport Category Airplanes. Federal Aviation Administration.

[24] MIL-STD-1530C. DoD Standard Practice, Aircraft Structural Integrity Program (ASIP). Aeronautical Systems Center, Wright-Patterson AFB, Ohio, 2005.

[25] Defence Standard 00-970. Design and Airworthiness Requirements for Service Aircraft. 1 - Fixed Wing Section 3 - Structure. UK Ministry of Defence.

[26] T. Belytschko, W. K. Liu, and B. Moran. Nonlinear finite elements for continua and structures. Wiley, Chichester, 2000.

[27] J. N. Reddy. Mechanics of laminated composite plates and shells: theory and analysis. CRC Press, Second edition, Boca Raton, 2004.

[28] H. T. Hahn and S. W. Tsai. Nonlinear elastic behavior of unidirectional composite laminates. Journal of Composite Materials, 7(1):102–118, 1973.

[29] A. C. Orifici, I. Herszberg, and R. S. Thomson. Review of methodologies for composite material modelling incorporating failure. Composite Structures, 86(1-3):194–210, 2008.

[30] M. J. Hinton, A. S. Kaddour, and P. D. Soden. Failure criteria in fibre-reinforced polymer composites. Elsevier, Oxford, 2004.

[31] R. Hill. The mathematical theory of plasticity. Oxford University Press, Oxford, 1950.

[32] V. D. Azzi and S. W. Tsai. Anisotropic strength of composites. Experimental Mechanics, 5(9):283–288, 1965.

[33] L. J. Hart-Smith. The role of biaxial stresses in discriminating between meaningful and illusory composite failure theories. McDonnell Douglas Corporation, Long Beach, 1991.

[34] S. W. Tsai and E. M. Wu. General theory of strength for anisotropic materials. Journal of Composite Materials, 5:58–80, 1971.

[35] R. M. Christensen. Mechanics of composite materials. Dover Publications, New York, 2005.

[36] Z. Hashin and A. Rotem. A fatigue failure criterion for fiber reinforced materials. Journal of Composite Materials, 7:448–464, 1973.

[37] Z. Hashin. Failure criteria for unidirectional fibre composites. Journal of Applied Mechanics, 47:329–34, 1980.

[38] S. E. Yamada and C. T. Sun. Analysis of laminate strength and its distribution. Journal of Composite Materials, 12(3):275–284, 1978.

[39] F. K. Chang and K. Y. Chang. A progressive damage model for laminated composites containing stress concentrations. Journal of Composite Materials, 21(9):834–55, 1987.

[40] F. K. Chang and L. B. Lessard. Damage tolerance of laminated composites containing an open hole and subject to compressive loadings: Part I - analysis. Journal of Composite Materials, 25(1):2–43, 1991.

[41] A. Olmedo and C. Santiuste. On the prediction of bolted single-lap composite joints. Composite Structures, 94(6):2110–2117, 2012.

[42] C. G. Davila, P. P. Camanho, and C. A. Rose. Failure criteria for frp laminates. Composites Part A: Applied Science and Manufacturing, 39(4):323–345, 2005.

[43] S. T. Pinho, C. G. Davila, P. P. Camanho, L. Iannucci, and P. Robinson. Failure models and criteria for FRP under in-plane or three-dimensional stress states including shear non-linearity. NASA/TM-2005-213530, Hampton, 2005.

[44] J. Zhang and J. Rowland. Damage modeling of carbon-fiber reinforced polymer composite pin-joints at extreme temperatures. Composite Structures, 94(8):2314–2325, 2012.

[45] K. I. Tserpes, G. Labeas, P. Papanikos, and Th. Kermanidis. Strength prediction of bolted joints in graphite/epoxy composite laminates. Composites Part B: Engineering, 33:521–529, 2002.

[46] S. C. Tan. A progressive failure model for composite laminates containing openings. Journal of Composite Materials, 25(5):556–577, 1991.

[47] P. P. Camanho and F. L. Matthews. A progressive damage model for mechanically fastened joints in composite laminates. Journal of Composite Materials, 33(24):2248–2280, 1999.

[48] M. L. Dano, E. Kamal, and G. Gendron. Analysis of bolted joints in composite laminates: Strains and bearing stiffness predictions. Composite Structures, 79(4):562–570, 2007.

[49] P. Maimi, P. P. Camanho, J. A. Mayugo, and C. G. Davila. A continuum damage model for composite laminates: Part I - constitutive model. Mechanics of Materials, 39(10):897–908, 2007.

[50] P. Maimi, P. P. Camanho, J. A. Mayugo, and C. G. Davila. A continuum damage model for composite laminates: Part II - computational implementation and validation. Mechanics of Materials, 39(10):909–919, 2007.

[51] I. Lapczyk and J. A. Hurtado. Progressive damage modeling in fiber-reinforced materials. Composites Part A: Applied Science and Manufacturing, 38(11):2333–2341, 2002.

[52] S. T. Pinho, L. Iannucci, and P. Robinson. Physically-based failure models and criteria for laminated fibre-reinforced composites with emphasis on fibre kinking: Part I: Development. Composites Part A: Applied Science and Manufacturing, 37(1):63–73, 2006.

[53] S. T. Pinho, L. Iannucci, and P. Robinson. Physically-based failure models and criteria for laminated fibre-reinforced composites with emphasis on fibre kinking: Part II: FE implementation. Composites Part A: Applied Science and Manufacturing, 37(5):766–777, 2006.

[54] ABAQUS. Analysis user's manual, version 6.11., 2011. Dassault Systemes, Providence.

[55] T. J. R. Huges. The finite element method - Linear static and dynamic finite element analysis. Dover Publications, New York, 2000.

[56] R. D. Cook, D. S. Malkus, M. E. Plesha, and R. J. Witt. Concepts and applications of finite element analysis. John Wiley, Hoboken, 2002.

[57] F. L. Matthews, G. A. O. Davies, D. Hitchings, and C. Soutis. Finite element

modelling of composite materials and structures. Woodhead Publishing, Cambridge, 2000.

[58] O. O. Ochoa and J. N. Reddy. Finite element analysis of composite laminates. Kluwer Academic Publishers, Waterloo, 1992.

[59] P. P. Camanho and F. L. Matthews. Stress analysis and strength prediction of mechanically fastened joints in frp: a review. Composites Part A: Applied Science and Manufacturing, 28(6):529–547, 1997.

[60] M. L. Dano, G. Gendron, and A. Picard. Stress and failure of mechanically fastened joints in composite laminates. Composite Structures, 50(3):287–296, 2000.

[61] Y. Xiao and T. Ishikawa. Bearing strength and failure behavior of bolted composite joints (Part II: modeling and simulation). Composites Science and Technology, 65(7-8):1032–1043, 2005.

[62] C. Hühne, A. K. Zerbst, G. Kuhlmann, C. Steenbock, and R. Rolfes. Progressive damage analysis of composite bolted joints with liquid shim layers using constant and continuous degradation models. Composite Structures, 92(2):189–200, 2010.

[63] C. T. McCarthy, M. A. McCarthy, and V. P. Lawlor. Progressive damage analysis of multi-bolt composite joints with variable bolt-hole clearances. Composites Part B: Engineering, 36(4):290–305, 2005.

[64] P. Linde, J. Pleitner, H. De Boer, and C. Carmone. Modelling and simulation of fiber metal laminates. In ABAQUS Users Conference, Boston, 2004.

[65] T. Ireman. Three-dimensional stress analysis of bolted single-lap composite joints. Composite Structures, 43(3):195–216, 1998.

[66] F. Rosales-Iriarte, N. A. Fellows, and J. F. Durodola. Failure prediction in carbon composites subjected to bearing versus bypass loading. Journal of Composite Materials, 46(15):1859–1878, 2012.

[67] B. Egan, C. T. McCarthy, M. A. McCarthy, P. J. Gray, and R. M. Frizzell. Modelling a single-bolt countersunk composite joint using implicit and explicit finite element analysis. Computational Materials Science, 64:203–208, 2012.

[68] M. Chishti, C. H. Wang, R. S. Thomson, and A. C. Orifici. Numerical analysis of damage progression and strength of countersunk composite joints. Composite Structures, 94(2):643–653, 2012.

[69] T. Ireman, R. Ranvik, and I. Eriksson. On damage development in mechanically fastened composite laminates. Composite Structures, 49(2):151–171, 2000.

[70] J. Schön. Coefficient of friction for aluminum in contact with a carbon fiber epoxy composite. Tribology International, 33(5):395–404, 2004.

[71] R. de Borst, M. A. Chrisfield, J. J. C. Remmers, and C. V. Verhoosel. Nonlinear finite element analysis of solids and structures. John Wiley, Second edition, Chichester, 2012.

[72] S. Weyer, H. Hooputra, and F. Zhou. Modeling of self-piercing rivets using fasteners in crash analysis. In ABAQUS Users Conference, Boston, 2006.

[73] P. J. Gray and C. T. McCarthy. A global bolted joint model for finite element analysis of load distributions in multi-bolt composite joints. Composites Part B: Engineering, 41(4):317–325, 2010.

[74] P. J. Gray and C. T. McCarthy. A highly efficient user-defined finite element for load distribution analysis of large-scale bolted composite structures. Composites Science and Technology, 71(12):1517–1527, 2011.

[75] J. Ekh and J. Schön. Finite element modeling and optimization of load transfer in multi-fastener joints using structural elements. Composite Structures, 82(2):245–256, 2008.

[76] A. J. Wang and K. F. Chung. Advanced finite element modelling of perforated composite beams with flexible shear connectors. Engineering Structures, 30(10):2724–2738, 2008.